PRE–EQUALIZATION FOR PRE-RAKE MISO DS–UWB SYSTEMS

by

Elham Torabi

B.A.Sc., University of Tehran, 1997

A THESIS SUBMITTED IN PARTIAL FULFILLMENT OF
THE REQUIREMENTS FOR THE DEGREE OF

MASTER OF APPLIED SCIENCE

in

THE FACULTY OF GRADUATE STUDIES

(Electrical and Computer Engineering)

THE UNIVERSITY OF BRITISH COLUMBIA

November 2007

Abstract

In recent years, ultra–wideband (UWB) communications has gained tremendous popularity in both research community and industry. The large bandwidth of UWB systems raises new wireless channel effects and consequently unique advantages as well as challenges to be dealt with, compared to conventional wireless systems. One of these advantages is the ability to resolve dense multipath components and use Rake combining at the receiver in order to significantly reduce the negative effects of fading. However, implementing a Rake receiver with a sufficiently large number of fingers to make use of this advantage is an evident challenge for most UWB devices with limited signal processing capabilities. A possible approach to overcome this problem is to move computational complexity from the receiver to the more powerful transmitter, which is the main focus of the present work.

In this thesis, we propose two novel pre–equalization schemes for multiple–input single–output (MISO) direct–sequence ultra–wideband (DS–UWB) systems with pre–Rake combining and symbol–by–symbol detection. The first pre–equalization filter (PEF) scheme employs one PEF per transmit antenna, whereas in the second, simplified PEF (S–PEF) scheme all transmit antennas share the same PEF. For both schemes the optimum finite impulse response (FIR) and infinite impulse response (IIR) PEFs are calculated based on the minimum mean squared error (MMSE) criterion. We show that in contrast to previously proposed schemes for DS–UWB, both our proposed PEF schemes efficiently exploit the channel shortening properties of the pre–Rake filter. In

particular, our proposed PEF schemes operate at the symbol level. We also show that under certain conditions the S–PEF scheme achieves the same performance as the more complex PEF scheme. Finally, we demonstrate that a single–input multiple–output (SIMO) DS–UWB system with post–Rake combining and MMSE post–equalization is the dual system to the considered MISO DS–UWB system with pre–Rake combining and MMSE pre–equalization. This uplink–downlink duality can be exploited for efficient calculation of the PEFs and for complexity reduction.

Our simulation results show that the proposed PEF schemes achieve significant performance gains over pre–Rake combining without equalization even if only short PEFs are employed, and this is the case even for long UWB channel impulse responses.

Contents

List of Figures

List of Abbreviations and Symbols

Acronyms

A–pre–Rake	All–pre–Rake
AWGN	Additive white Gaussian noise
BER	Bit error rate
CIR	Channel impulse response
CSI	Channel state information
DS	Direct–sequence
FH	Frequency hopping
FIR	Finite impulse response
IIR	Infinite impulse response
ISI	Intersymbol interference
LOS	Line–of–sight
MF	Matched filter
MISO	Multiple–input single–output
MMSE	Minimum mean-square error
OFDM	Orthogonal frequency division multiplexing
OOK	On–off keying
PAM	Pulse–amplitude modulation

pdf	Probability density function
PHY	Physical–layer
PPM	Pulse–position modulation
P–pre–Rake	Partial–pre–Rake
PSD	Power spectral density
PSK	Phase–shift keying
PEF	Pre–equalization filter
PSK	Phase shift keying
RV	Random variable
SIMO	Single–input multiple–output
SISO	Single–input single–output
SNR	Signal–to–noise ratio
S–PEF	Simplified pre–equalization filter
S–pre–Rake	Selective–pre–Rake
UWB	Ultra–Wideband
WPAN	Wireless Personal Area Network

Operators and Notation

$\mathrm{diag}\{\cdot\}$	(Block) diagonal matrix
$\mathcal{E}\{\cdot\}$	Statistical expectation
$(\cdot)^*$	Complex conjugation
$(\cdot)^{1/2}$	Matrix square root
$[\cdot]^T$	Matrix or vector transposition
$[\cdot]^H$	Matrix or vector Hermitian transposition
$\lvert\cdot\rvert$	Absolute value of a complex number
$\mathbf{0}_X$	X–dimensional all–zeros column vector
$\boldsymbol{I}_X$	$X \times X$ Identity matrix

$\boldsymbol{e}_n$	Unit vector whose elements are all zero except the nth element which is equal to 1
$\Re\{\cdot\}$	Real part of a complex number
$*$	Linear convolution
$\delta(\cdot)$	Dirac delta function
$Q(x)$	Gaussian Q–function
$X(e^{j\omega})$	Discrete–time Fourier transform of sequence $x[k]$
$\mathcal{F}\{x[k]\}$	Discrete–time Fourier transform

Acknowledgments

I would like to express my sincere gratitude to Dr. Robert Schober who encouraged me at every stage of my research. This thesis could not have been completed without his invaluable guidance and continuous support. Undoubtedly, his priceless suggestions and helpful feedback has improved the quality of this work in every aspect. I would also like to extend my appreciation to Dr. Jan Mientzner for his significant contribution and helpful comments and his generosity in devoting his time to review this thesis.

I am sincerely grateful to my family for their constant encouragement and especially my husband Farshid for his unwavering support and understanding.

Furthermore, I would like to thank all my colleagues at the Department of Electrical and Computer Engineering at UBC, for creating a stimulating and friendly environment.

Elham Torabi

Chapter 1

Introduction

The following section provides a short overview of ultra–wideband (UWB) technology. In the next section, the background and motivation for the present work is summarized, and a short history of previously proposed related works is provided. The third section of this chapter briefly summarizes the contributions of this work, and the last section outlines the organization of the thesis.

1.1 UWB Technology

Ultra–wideband (UWB) radio is a rapidly emerging technology with attractive and promising features for wireless communications such as wireless personal area networks (WPANs), imaging, radar, and positioning systems [1]. In February 2002, the Federal Communications Commission (FCC) allocated 7.5 MHz of spectrum (3.1 to 10.6 GHz frequency band) for unlicensed use of UWB technology, which resulted in a rapidly growing research interest in this field in academia and industry. The strict power limitations ruled by FCC determined two different suitable application categories for UWB communications. The first one is high bit rate applications over short ranges. The

IEEE 802.15.3a Task Group (TG) was an exemplary attempt to standardize this category. The second category regulates low bit rate applications over medium-to-long ranges, dealt with in the IEEE 802.15.4a TG [2]. The focus of the present work is on high bit rate UWB applications. The FCC spectral mask, shown in Fig. 1.1 allows indoor UWB communications to coexist with other technologies with power spectral densities (PSDs) not exceeding -41.3 dBm/MHz [3]. Fig. 1.1 shows the allowed level of effective isotropic radiated power (EIRP) of the UWB transmitting antenna. A common method to maintain the FCC power spectrum mask for a given data rate is to limit the energy per pulse by proper pulse waveform design, and reducing the transmit power for a fixed pulse waveform. According to the modern definition, UWB refers

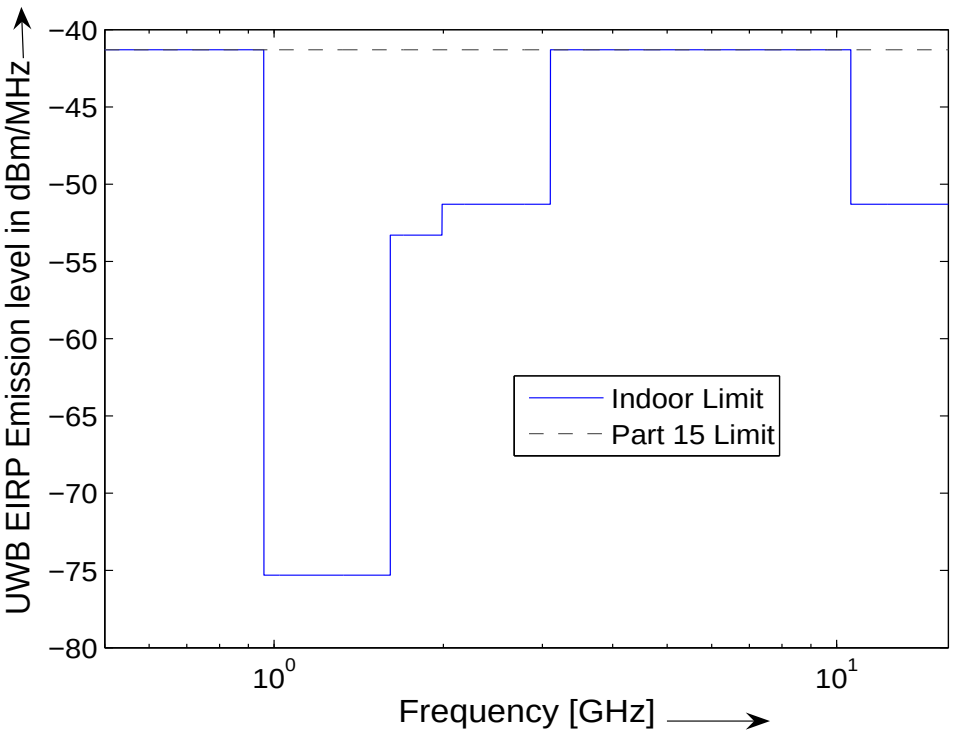

Figure 1.1: UWB spectral mask and FCC part 15 limits.

to any wireless transmission with instantaneous spectral occupancy of more than 500 MHz or a fractional bandwidth greater than 20%. The fractional

bandwidth B_f is mathematically defined as

$$B_f = \frac{B}{f_c} = \frac{f_H - f_L}{f_c}, \tag{1.1}$$

where $B = f_H - f_L$ denotes the -10 dB bandwidth and $f_c = (f_H + f_L)/2$ is the center frequency, with f_H being the upper frequency of the -10 dB emission point, and f_L being the lower frequency of the -10 dB emission point. UWB systems with $f_c > 2.5$ GHz need to have a -10 dB bandwidth of at least 500 MHz, and UWB systems with $f_c < 2.5$ GHz need fractional bandwidth of at least 0.2 [4].

There are two main candidates for UWB physical–layer (PHY). One candidate is multiband orthogonal frequency division multiplexing (MB–OFDM), which is based on the transmission of continuous OFDM signals combined with frequency hopping (FH) over instantaneous frequency bandwidths of 528 MHz. The second strong candidate is known as direct–sequence (DS) UWB, and is based on transmission of UWB DS-coded pulses, which are extremely short (in the order of nanoseconds) and of low power [2]. In the present work, we consider carrier modulated DS–UWB which was also considered for standardization in the IEEE 802.15.3a TG. However, we do not restrict our work to any standard. Various types of modulations can be employed for DS–UWB, including on–off keying (OOK), pulse–amplitude modulation (PAM), pulse–position modulation (PPM), and phase–shift keying (PSK), as well as different receiver types such as the energy detector [5], differential detector [6], Rake receiver [7], and transmitted reference receiver [8].

The well–known advantages of UWB systems can be summarized as unlicensed usage of an extremely wideband spectrum, great flexibility of spectrum usage, and capability of implementing adaptive transceivers for trade–off between data rate, range, power, and quality-of-service within the same hardware. UWB high temporal resolution, implies robustness against multipath fading, and low fading margin requirements. Finally, ranging capabilities, low power transmission, and robustness against eavesdropping are other advantages of

UWB systems [2].

1.2 Background and Motivation

As their unique characteristic, UWB systems can resolve even dense multipath components, due to their extremely large bandwidths such that Rake combining can be used at the receiver to efficiently capture energy and significantly reduce the negative effects of fading in the received signal [9, 10]. However, the implementation of the receiver, requires a Rake receiver and can be considerably complex in a multipath environment. Digital implementation of the Rake receiver requires very high sampling and processing speed, both during the channel estimation and the actual data reception. However, for many UWB applications the receiver is a portable device with severely limited signal processing capabilities making the implementation of Rake combiners with a sufficiently large number of fingers very challenging.

A promising approach to overcome this problem is to move computational complexity from the receiver to the more powerful transmitter (e.g. an access point). For this purpose the concept of pre–Rake combining (also referred to as time–reversal) was borrowed from other areas such as time–division duplex code–division multiple access (TDD–CDMA) systems [11] and underwater acoustic communication [12], and was modified for UWB applications, cf. e.g. [13]–[21]. Pre–Rake combining exploits the reciprocity of the UWB channel which was recently experimentally confirmed in [19]. Ideally, with pre–Rake combining channel estimation, diversity combining, and equalization are avoided at the receiver, and a simple symbol–by–symbol detector can be used [14, 20]. In addition, it has recently been shown that pre–Rake combining also performs well in the presence of multiple users [17], and the extension to multiple–input single–output (MISO) scenarios was proposed in [17, 19].

Despite all of these desirable properties, pre–Rake combining has a serious

drawback. In particular, for the long channel impulse responses (CIRs), which are typical for UWB applications, it may entail a relatively high error floor if simple symbol–by–symbol detection is applied [15, 13]. To remedy this problem receiver–side equalization [22, 13, 23] and post–Rake combining [18] have been proposed. However, these techniques increase the receiver complexity and thus, compromise to some extend the advantages of pre–Rake combining. Therefore, transmitter–side approaches for performance improvement seem to be more suitable for pre–Rake UWB systems. One option in this regard is to decrease the data rate (i.e., increase the chip or/and symbol duration), which effectively decreases the residual intersymbol interference (ISI) at the receiver [20]. However, if high data rates are desired, some form of pre–equalization has to be applied at the transmitter. In [24] the pre–Rake filter is replaced by a pre–filter which minimizes the residual ISI at the receiver based on the minimum mean squared error (MMSE) criterion. Since this MMSE pre–filter is implemented at the chip level, depending on the underlying channel, relatively long filters may be necessary to achieve a good performance. This entails a high complexity, since the computation of the filter coefficients requires the inversion of a matrix with a size equal to the filter length.

1.3 Contributions

In this thesis, we propose a novel pre–equalization filter (PEF) scheme for MISO DS–UWB systems which consists of a bank of pre–Rake filters and a bank of PEFs. Unlike [24], we retain the pre–Rake filters, as they efficiently shorten the overall CIRs, and implement the PEFs at the symbol level. As a result, the PEF lengths required to achieve certain performance are much smaller for the proposed scheme than for the scheme in [24], leading to a lower complexity for filter computation. Although pre–equalization problems have been extensively studied in the literature, e.g. [25, 26], existing results cannot

be easily adopted for the problem at hand due to the presence of the pre–Rake, the imposed simple receiver processing, and the spreading applied in DS–UWB.

The main contributions of the present research work are as follows:

- We derive a closed–form solution for the optimum finite impulse response (FIR) and infinite impulse response (IIR) MMSE PEF coefficients for the MISO DS-UWB system. The MMSE criterion for optimization is minimizing the error variance at the receiver while limiting the power of the transmitted signal over one symbol interval. We also analyze the performance of the resulting system. Our simulation results confirm that the proposed PEF scheme achieves significant performance gains over pre–Rake structures without equalization and that the performance of IIR PEFs can be closely approached by relatively short FIR PEFs, even for long UWB CIRs. We compare our simulation results with analytical Gaussian approximation results and show that they are in good agreement for a sufficient number of filter coefficients.
- We discuss the optimality of all–pre–Rake (A–pre–Rake), and show in detail that increasing the spreading factor N decreases the error variance by decreasing the effective spectral fluctuation for a given number of antennas, and consequently improves the system performance. Simulation results also show that increasing the number of antennas has a similar positive effect, while providing an additional combining gain, which leads to better system performance.
- As a meaningful performance bound for any (pre–)equalizer and any (pre–)Rake scheme, matched–filter (MF) bounds are derived for our proposed schemes. It is mathematically shown that, for the proposed PEF scheme, as the spreading factor N tends to infinity the effective signal-to-noise ratio (SNR) becomes the same as the resulting SNR for the equivalent matched–filtered system.

- We show that a single–input multiple–output (SIMO) system with post–Rake combining followed by MMSE equalization is the dual system to the proposed MISO system with pre–Rake combining and pre–equalization. This uplink–downlink duality [27] can be conveniently exploited for efficient adaptive computation of the PEFs. A practical implications for the uplink–downlink duality is that, while adaptive algorithms cannot be used to calculate the optimum downlink filter (since the received signal is not available at the transmitter) algorithms such as the least–mean square (LMS) or the recursive least squares (RLS) algorithm can be used to calculate optimum uplink filter efficiently, and from there, the optimum downlink filters can be easily obtained.
- We also propose a simplified PEF (S–PEF) scheme for the MISO system, where the bank of PEFs is replaced by a single PEF. We demonstrate that, under certain conditions, the S–PEF scheme can achieve the same performance as the more complex PEF scheme. The simulation results show that for sufficient, but still relatively small numbers of FIR PEF coefficients, the PEF scheme can be replaced by the S–PEF scheme without significant loss in system performance.
- Since we assume perfect channel state information (CSI) in all our derivations and analysis, we briefly study the effect of having imperfect CSI at the transmitter on the performance of the proposed schemes. Simulation results show that our proposed schemes are reasonably robust and not very sensitive to CSI errors. We also observe that channels with longer delay spreads are more sensitive to CSI errors, however.

The results of our work are summarized in the following papers:

- E. Torabi, J. Mietzner, and R. Schober. Pre-Equalization for MISO DS–UWB Systems with Pre–Rake Combining. *Accepted subject to minor revisions in the IEEE Transactions on Wireless Communications*, Oct. 2007.

- E. Torabi, J. Mietzner, and R. Schober. Pre-Equalization for Pre–Rake MISO DS–UWB Systems. *Submitted to the IEEE International Conference on Communications (ICC)*, Aug. 2007.

1.4 Thesis Organization

In Chapter 2, we present the considered transmitter structure, channel model, and receiver structure. The proposed PEF scheme is optimized and analyzed for both the FIR and the IIR case in Chapter 3. The uplink–downlink duality is covered in Chapter 4, and the S–PEF scheme is investigated in Chapter 5. In Chapter 6, we compare the performances of the PEF scheme and the S-PEF scheme for IIR cases, and briefly discuss the pre–filtering method proposed in [24] in order to compare its performance with that of our proposed methods. In Chapter 7, simulation results are provided, and Chapter 8 concludes this thesis.

Chapter 2

System and Channel Model

In this thesis, we consider a MISO DS–UWB system with M transmit antennas, symbol duration T_s, and chip duration $T_c = T_s/N$, where N is the spreading factor. A block diagram of the discrete–time model of this system is shown in Fig. 2.1. We note that our results could be extended to multiple receive antennas in a straightforward fashion. However, for the sake of clarity and since a simple receiver structure is desired, we assume that only a single receive antenna is available. To emphasize the different capabilities of the transmitter and the receiver we will also refer to the system in Fig. 2.1 as the *downlink*. Furthermore, for convenience, all signals and systems are represented by their complex baseband equivalents. In the following, the transmitter structure of the proposed PEF scheme, the adopted channel model, correlated shadowing, and the receiver structure are discussed.

2.1 Transmitter Structure

At antenna m, $1 \leq m \leq M$, the transmitted independent and identically distributed (i.i.d.) data symbols $a[n] \in \{\pm 1\}$ are filtered with a PEF $f_m[n]$ of

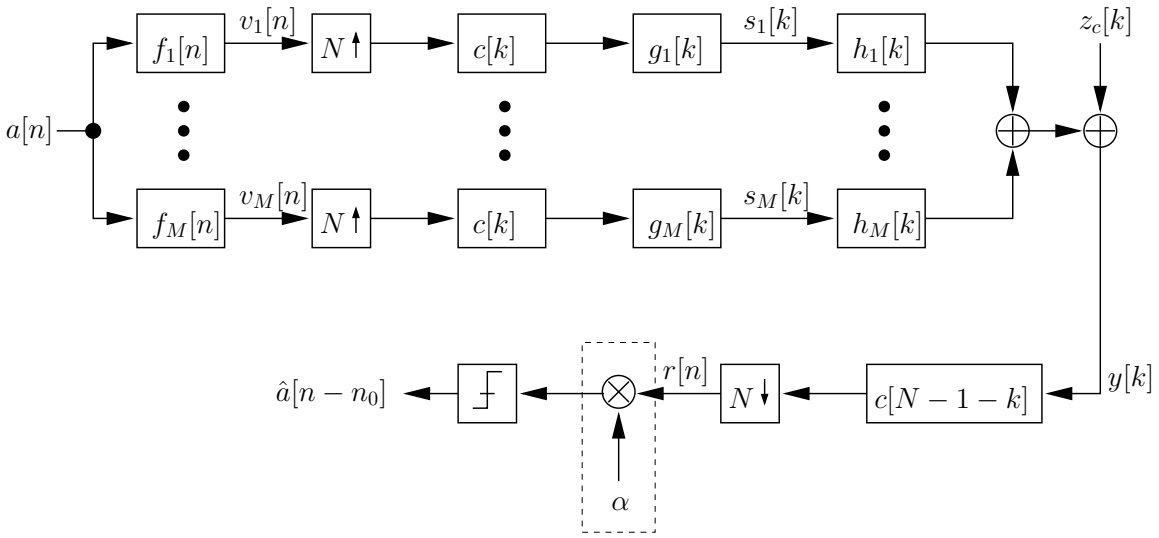

Figure 2.1: Block diagram of a MISO DS–UWB system (downlink) with M transmit antennas, pre–Rake combining, and pre–equalization. The multiplication of $r[n]$ with α (dashed box) does not have to be implemented at the receiver, cf. discussion in Section 2.3 and Chapter 3.

length L_f. The filter output signal

$$v_m[n] \triangleq f_m[n] * a[n] = \sum_{l=0}^{L_f-1} f_m[l]a[n-l] \tag{2.1}$$

is up–sampled by a factor of N. The up–sampled signal is then filtered with a (real–valued) spreading sequence $c[k]$, $0 \leq k < N$, and with a pre–Rake filter $g_m[k]$ of length L_g. For convenience the spreading sequence is normalized to $\sum_{k=0}^{N-1} |c[k]|^2 = 1$. The resulting transmit symbol $s_m[k]$ is given by

$$s_m[k] = \sum_{i=-\infty}^{\infty} v_m[i]\tilde{g}_m[k-iN], \tag{2.2}$$

where $\tilde{g}_m[k] \triangleq c[k] * g_m[k]$ includes the combined effects of the pre–Rake filter and the spreading. We note that the considered transmitter structure is very general as we do not impose any restrictions on $c[k]$ and $g_m[k]$. If a spreading sequence is not applied, e.g. [13, 17, 19, 24], $c[0] = 1$ and $c[k] = 0$, $1 \leq k < N$.

In general, $g_m[k]$, $1 \leq m \leq M$, will depend in some way on the CIR $h_m[k]$, which is of length L_h. For example, for an all–pre–Rake (A–pre–Rake or time–

reversal filter) $g_m[k]$ is given by

$$g_m[k] \triangleq \begin{cases} h_m^*[L_h - k - 1], & 0 \leq k < L_g, \\ 0, & \text{otherwise}, \end{cases} \tag{2.3}$$

where $L_g = L_h$, for a partial–pre–Rake (P–pre–Rake) we have

$$g_m[k] \triangleq \begin{cases} h_m^*[L_g - k - 1], & 0 \leq k < L_g, \\ 0, & \text{otherwise}, \end{cases} \tag{2.4}$$

where $L_g < L_h$, and a selective pre–Rake (S–pre–Rake) is defined by

$$g_m[k] \triangleq \begin{cases} h_m^*[L_g - k - 1], & 0 \leq k < L_g, \\ 0, & \text{otherwise}, \end{cases} \tag{2.5}$$

for the S largest coefficients of $h_m[k]$, where $L_g \leq L_h$ may be adopted [28].

Since for typical UWB CIR lengths it is not realistic to assume that the CIR coefficients can be fed back from the receiver to the transmitter [21], as any UWB transmitter structure requiring CSI, the proposed PEF scheme hinges on the reciprocity of the UWB channel and the use of time–division duplex (TDD) is assumed, in which the same frequency band is used for both the uplink and downlink by switching between transmission and reception in time. Fortunately, this reciprocity has been experimentally confirmed [19]. Hence, $h_m[k]$ can be estimated at the transmitter relieving the receiver from any channel estimation tasks.

2.2 Channel Model

The equivalent baseband discrete–time CIRs $h_m[k] \triangleq g_T(t) * h_m(t) * g_R(t)|_{kT_c}$, $1 \leq m \leq M$, contain the combined effects of the transmit filter $g_T(t)$, the continuous–time CIR $h_m(t)$, and the receive filter $g_R(t)$. Furthermore, for the wireless channel we adopt the recently proposed extension of the IEEE 802.15.3a channel model [29, 30] to multiple antennas [31]. Consequently, the

passband version $h'_m(t)$ of the baseband CIR $h_m(t)$ consists of L_c clusters of L_r rays [32] and is modeled as

$$h'_m(t) = X_m \sum_{l=1}^{L_c} \sum_{k=1}^{L_r} \alpha_{k,l,m} \delta(t - T_{l,m} - \tau_{k,l,m}), \tag{2.6}$$

where $T_{l,m}$ is the delay of the lth cluster, $\tau_{k,l,m}$ is the delay of the kth ray of the lth cluster, $\alpha_{k,l,m}$ is the random multipath gain coefficient, and X_m models the log–normal shadowing and can be represented as

$$X_m = 10^{\frac{\sigma_x}{20} w_m}, \tag{2.7}$$

where σ_x is the standard deviation for log–normal shadowing in dB and is assumed to be 3 dB as given in [29], and the variable w_m is defined as a Gaussian random variable (RV) with zero–mean and unit variance, i.e., $w_m \sim N(0, 1)$. In [29, 30] four parameter sets for the various channel model parameters in Eq. (2.6) are specified. The resulting four channel models (CMs) are known as CM1, CM2, CM3, and CM4 and represent different usage scenarios. CM1 describes a line–of–sight (LOS) scenario with a separation between transmitter and receiver of less than 4 m. CM2 describes the same range, but for a non–LOS situation. CM3 describes a non–LOS scenario for distances of 4-10 m between transmitter and receiver. Finally, CM4 describes an environment with strong delay dispersion, resulting in a delay spread of 25 ns [29, 30]. For the simulations provided in this work, we consider CM1 and CM4, which have the shortest and the longest delay spread, respectively. As an example, 100 CIR realizations for CM1 and CM4 are shown in Fig. 2.2 and Fig. 2.3, respectively. Later on, in Chapter 7, we will show how the long delay spread of UWB channels can affect the system performances.

Measurements reported in [31] have confirmed that while $T_{l,m}$, $\tau_{k,l,m}$, and $\alpha_{k,l,m}$ are independent across antennas, the log–normal terms X_m are mutually correlated. Adequate modeling of correlated shadowing in UWB MIMO channels is a pre-requisite to achieve an accurate performance analysis. Based on [31], a recently proposed modeling method for correlated shadowing with

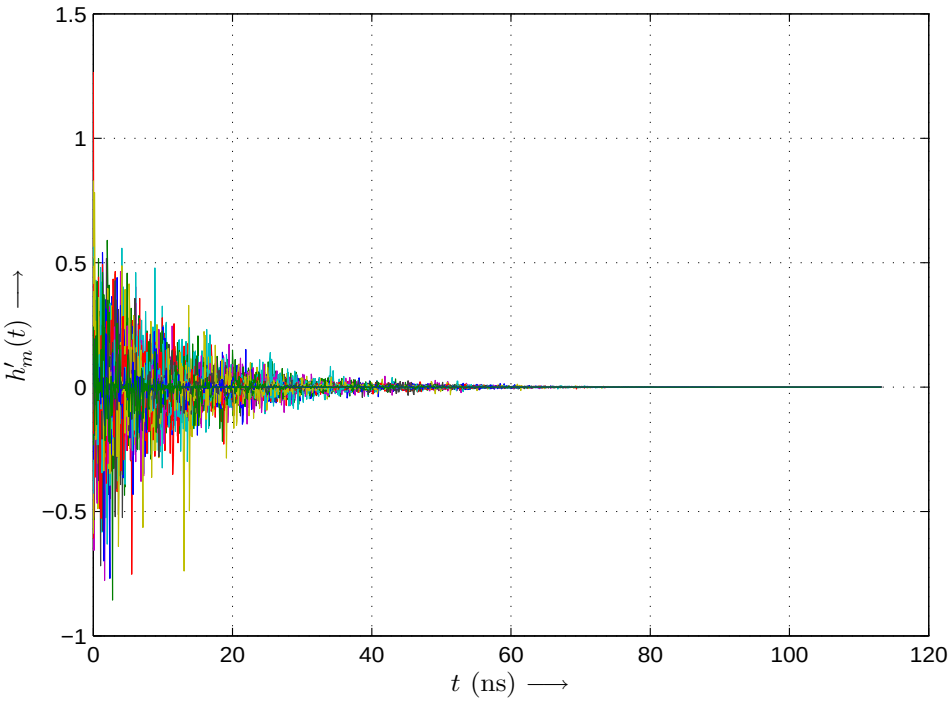

Figure 2.2: 100 CIR realizations for CM1.

log-normal distribution in UWB MIMO channels and the IEEE 802.15.3a channel model is used in the present work. As mentioned earlier we assume a UWB MISO channel with M transmit antennas, therefore we focus our derivations to UWB MISO channel. The goal is to relate correlation coefficients for log–normal distributed RV X_m to the correlation coefficients for their corresponding Gaussian distributed RV w_m. Let $\boldsymbol{x} = [X_1, X_2, \cdots, X_M]^T$ be the vector of correlated shadowing RVs, with X_m defined according to Eq. (2.7). Since the log–normal distributed RVs X_m, $1 \leq m \leq M$ are correlated, their corresponding Gaussian RVs w_m, $1 \leq m \leq M$ are correlated as well. We assume vector $\boldsymbol{w} = [w_1, w_2, \cdots, w_M]^T$ as a joint Gaussian distribution with correlation matrix defined as $\boldsymbol{R}_{T_w} = [\rho_{w_m,w_n}]_{M\times M}$, where ρ_{w_m,w_n} denotes the correlation coefficient and is defined as

$$\rho_{w_m,w_n} = \mathcal{E}\left\{w_m \times w_n\right\}. \tag{2.8}$$

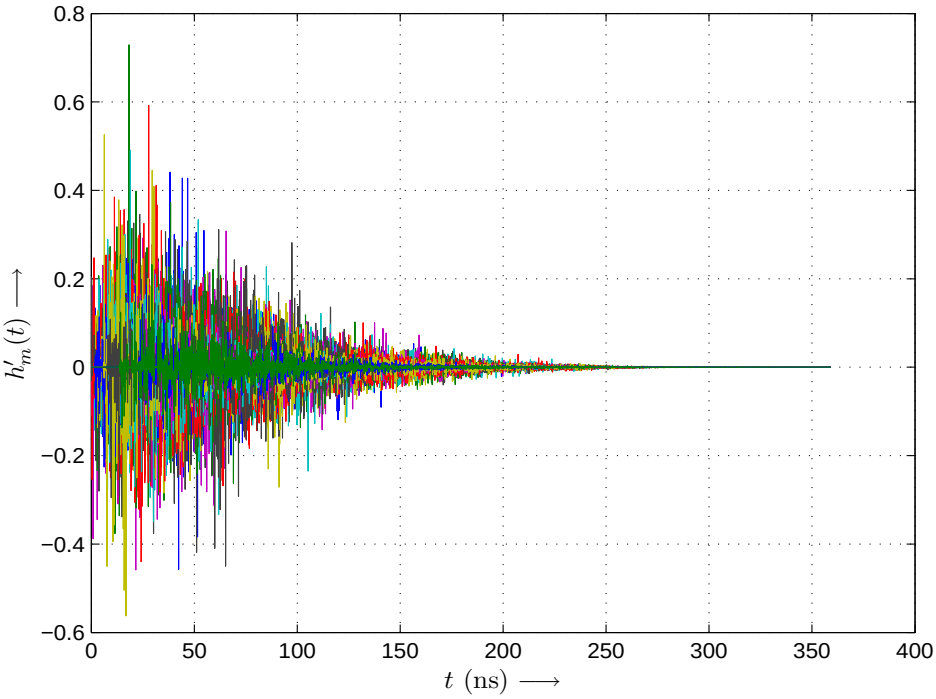

Figure 2.3: 100 CIR realizations for CM4.

The correlation coefficient for the log–normal RVs X_m and X_n can then be computed based on the Gaussian RVs w_m and w_n as [31]

$$\rho_{X_m,X_n} = \frac{e^{\lambda^2\sigma_x^2\rho_{w_m,w_n}} - 1}{e^{\lambda^2\sigma_x^2} - 1} \tag{2.9}$$

where $\lambda = \ln 10/20$. The correlation coefficient for the Gaussian RVs w_m and w_n can also be obtained as

$$\rho_{w_m,w_n} = \frac{1}{\lambda^2\sigma_x^2} \ln\left[\left(e^{\lambda^2\sigma_x^2} - 1\right)\rho_{X_m,X_n} + 1\right]. \tag{2.10}$$

If we assume that the correlation matrix for the log–normal shadowing $\boldsymbol{x}$ at the transmitter end is given by $\boldsymbol{R}_{T_x} = [\rho_{X_m,X_n}]_{M\times M}$, corresponding correlation matrix $\boldsymbol{R}_{T_w}$ for the Gaussian RVs $\boldsymbol{w}$ can be computed using Eq. (2.10).

In particular, the correlated Gaussian random vector $\boldsymbol{w}$ is obtained as

$$\boldsymbol{w} = (\boldsymbol{R}_{T_w})^{1/2}\,\boldsymbol{w}^{(u)} \tag{2.11}$$

where $\boldsymbol{w}^{(u)} = \left[w_1^{(u)}, w_2^{(u)}, \cdots, w_M^{(u)}\right]^T$ is defined as a random vector that consists of real–valued i.i.d. Gaussian RVs with zero–mean and unit variance. Eq. (2.11) ensures that the random vector $\boldsymbol{w}$ has the predefined correlation matrix $\boldsymbol{R}_{T_w}$.

We now conclude that the correlated shadowing for UWB MISO channels can be generated using Eq. (2.7), where the correlated real–valued Gaussian RV w_m can be modeled by Eq. (2.11). Finally, the correlation matrix $\boldsymbol{R}_{T_w}$ in terms of Gaussian distribution can be obtained from the correlation matrix $\boldsymbol{R}_{T_x}$ in terms of their corresponding log–normal distribution using Eq. (2.10). We will use these results in order to generate correlated channels for UWB MISO systems in our simulations.

2.3 Receiver Structure

Consider again the system model depicted in Fig. 2.1. The received signal $y[k]$ is filtered with the time–reversed spreading sequence $c[N-1-k]$, $0 \leq k < N$. It will then be sampled at times $k = Nn + k_0$, where $0 \leq k_0 < N$ denotes the sampling phase. The resulting receiver output signal $r[n]$ can be expressed as

$$r[n] = \sum_{m=1}^{M} \sum_{l=-\infty}^{\infty} q_m[Nl + k_0] v_m[n-l] + z_s[n], \tag{2.12}$$

with the overall CIR

$$q_m[k] \triangleq \tilde{g}_m[k] * \tilde{h}_m[k], \tag{2.13}$$

where,

$$\tilde{h}_m[k] \triangleq h_m[k] * c[N-1-k], \tag{2.14}$$

and symbol–level noise

$$z_s[n] = \sum_{i=0}^{N-1} c[i] z_c[N(n-1) + k_0 + i + 1], \tag{2.15}$$

where $z_c[k]$ denotes the chip–level additive white Gaussian noise (AWGN) with variance $\sigma_c^2 \triangleq \mathcal{E}\{|z_c[k]|^2\}$. Consequently, $z_s[n]$ is also AWGN with variance

$\sigma_s^2 \triangleq \mathcal{E}\{|z_s[n]|^2\} = \sigma_c^2 \sum_{i=0}^{N-1} |c[i]|^2 = \sigma_c^2$. Ideally, the sampling phase k_0 should be optimized to maximize the energy of $q_m[Nl + k_0]$. However, the number of operations required for finding the optimum k_0 may be prohibitive, especially for large N. Therefore, in practice, it may be preferable to consider suboptimum choices for k_0 which yield a good performance and can be easily found. For an A–pre–Rake combiner $q_m[k]$ will assume its maximum for $k = L_g + N - 2$. In order to capture this maximum in $q_m[Nl + k_0]$, we require $k_0 = k_0^s \triangleq L_g + N - 2 - N \lfloor (L_g + N - 2)/N \rfloor$. Through extensive simulations we found that k_0^s yields a close–to–optimum performance not only for A–pre–Rake combining but also for S– and P–pre–Rake combining as long as the number of fingers is sufficiently large. We note that the analytical results in this thesis are valid for any sampling phase k_0 but for our simulation results in Chapter 7 we have adopted $k_0 = k_0^s$.

Since the goal of the proposed UWB system design is to minimize receiver complexity in the downlink, no additional filtering is applied at the receiver and symbol decisions are made according to[1]

$$\hat{a}[n - n_0] = \text{sign}\{\Re\{r[n]\}\}, \tag{2.16}$$

where $\hat{a}[n - n_0]$ is the estimate for $a[n - n_0]$, n_0 denotes the decision delay, and $\text{sign}\{x\} = 1$ if $x \geq 0$ and $\text{sign}\{x\} = -1$ otherwise. As typical for equalization problems, the decision delay n_0 has to be optimized for performance maximization if causal pre–filters are desired.

[1]Note that the multiplication with α in Fig. 2.1 does not have to be implemented at the receiver, see discussion in Chapter 3.

Chapter 3

PEF Optimization and Performance Analysis

In this thesis, we adopt the MMSE criterion for optimization of the PEFs $f_m[n]$. In particular, our design goal is to minimize the error variance

$$\sigma_e^2 \triangleq \mathcal{E}\{|a[n-n_0] - \alpha r[n]|^2\}, \tag{3.1}$$

while limiting the power P of the transmitted signal over one symbol interval, i.e.,

$$P \triangleq \sum_{k=Nn}^{N(n+1)-1} \sum_{m=1}^{M} \mathcal{E}\{|s_m[k]|^2\} = 1, \qquad \forall n. \tag{3.2}$$

Here, α in Eq. (3.1) is an auxiliary variable that simplifies the optimization of the PEFs $f_m[n]$ but does not affect the symbol decisions according to Eq. (2.16). Note that similar constraint as in Eq. (3.2) is used in other techniques for UWB applications cf. e.g. [13]–[21]. Since UWB systems have to comply with the FCC power spectrum mask as discussed in Chapter 1, it is also of interest to introduce additional constraints on the power spectrum density of the transmitted signal, which is not considered in the present work and is open for future research.

In the following section, we derive the optimum FIR PEFs based on Eqs. (3.1)

and (3.2), and provide an expression for the corresponding minimum error variance. In Section 3.2 we find closed–form solution for the optimum IIR PEF coefficients with slightly different method than that of the FIR PEFs and obtain the corresponding minimum error variance. We analyze the performance of the proposed PEF scheme and provide an expression for its bit–error–rate (BER) performance in Section 3.3, followed by a discussion on the optimality of A–pre–Rake for IIR PEFs in Section 3.4. Section 3.5 provides a performance lower bound for the proposed PEF scheme, and finally in Section 3.6 the effect of large spreading factors on the performance of the proposed PEF scheme is investigated.

3.1 FIR Pre–Equalization Filters

For FIR PEF optimization it is convenient to first rewrite Eq. (2.12) as

$$\begin{aligned} r[n] &= \sum_{m=1}^{M} (\boldsymbol{Q}_m \boldsymbol{f}_m)^H \boldsymbol{a}[n] + z_s[n] \\ &= (\boldsymbol{Q}\boldsymbol{f})^H \boldsymbol{a}[n] + z_s[n], \end{aligned} \tag{3.3}$$

where $\boldsymbol{a}[n] \triangleq [a[n] \ \dots \ a[n - L_t + 1]]^T$, $\boldsymbol{f} \triangleq [\boldsymbol{f}_1^T \ \dots \ \boldsymbol{f}_M^T]^T$, $\boldsymbol{f}_m \triangleq [f_m[0] \ \dots \ f_m[L_f - 1]]^H$, $\boldsymbol{Q} \triangleq [\boldsymbol{Q}_1 \ \dots \ \boldsymbol{Q}_M]$, and $\boldsymbol{Q}_m$ denotes an $L_t \times L_f$ column–circulant matrix defined as

$$\boldsymbol{Q}_m = \begin{bmatrix} q_m[k_0] & 0 & \dots & 0 \\ q_m[N+k_0] & q_m[k_0] & \dots & \vdots \\ q_m[2N+k_0] & q_m[N+k_0] & \dots & 0 \\ \vdots & \vdots & \ddots & q_m[k_0] \\ q_m[N(L_q-1)+k_0] & q_m[N(L_q-2)+k_0] & \ddots & q_m[N+k_0] \\ 0 & q_m[N(L_q-1)+k_0] & \ddots & \vdots \\ \vdots & \vdots & \ddots & q_m[N(L_q-2)+k_0] \\ 0 & 0 & \dots & q_m[N(L_q-1)+k_0] \end{bmatrix}. \tag{3.4}$$

Here, $L_t \triangleq L_q + L_f - 1$ and $L_q = \lceil (L_g + L_h + 2N - 3)/N \rceil$ are the lengths of the impulse response of the overall system (including the PEFs) and the sampled overall CIR $q_m[Nn + k_0]$, respectively. Applying Eq. (3.3) in Eq. (3.1) yields

$$\sigma_e^2 = 1 + |\alpha|^2 \sigma_c^2 - \alpha \boldsymbol{f}^H \boldsymbol{q} - \alpha^* \boldsymbol{q}^H \boldsymbol{f} + |\alpha|^2 \boldsymbol{f}^H \boldsymbol{Q}^H \boldsymbol{Q} \boldsymbol{f}, \tag{3.5}$$

where $\boldsymbol{q} \triangleq \boldsymbol{Q}^H \boldsymbol{e}_{n_0}$, and $\boldsymbol{e}_{n_0}$th denotes the unit vector whose elements are all zero except for the n_0 element which is equal to one.

Now, we evaluate Eq. (3.2). Based on Eq. (2.2) for antenna m we obtain

$$\begin{aligned}
\mathcal{E}\{|s_m[k]|^2\} &= \mathcal{E}\left\{s_m[k] s_m[k]^*\right\} \\
&= \sum_{i=-\infty}^{\infty} \sum_{j=-\infty}^{\infty} \mathcal{E}\left\{v_m[i] v_m^*[j]\right\} \tilde{g}_m[k - iN] \tilde{g}_m^*[k - jN] \\
&= \sum_{i=-\infty}^{\infty} \sum_{j=-\infty}^{\infty} \left\{ \sum_{k=-\infty}^{\infty} \sum_{l=-\infty}^{\infty} f_m[k] f_m^*[l] \mathcal{E}\left(a[i-k] a^*[j-l]\right) \right\} \times \\
&\quad \tilde{g}_m[k - iN] \tilde{g}_m^*[k - jN] \\
&= \sum_{i=-\infty}^{\infty} \sum_{j=-\infty}^{\infty} \left\{ \sum_{k=-\infty}^{\infty} \sum_{l=-\infty}^{\infty} f_m[k] f_m^*[l] \delta\left[i - j - k + l\right] \right\} \times \\
&\quad \tilde{g}_m[k - iN] \tilde{g}_m^*[k - jN] \\
&= \sum_{i=-\infty}^{\infty} \sum_{j=-\infty}^{\infty} \left\{ \sum_{k=-\infty}^{\infty} f_m[k] f_m^*[i - j + l] \right\} \tilde{g}_m[k - iN] \tilde{g}_m^*[k - jN]
\end{aligned}$$

$$= \sum_{i=-\infty}^{\infty} \sum_{j=-\infty}^{\infty} \varphi_{ff}^{m}[i-j]\tilde{g}_m[k-iN]\tilde{g}_m^*[k-jN], \tag{3.6}$$

where $\varphi_{ff}^{m}[k] \triangleq f_m[k] * f_m^*[-k]$. Eq. (3.6) shows that $s_m[k]$ is a cyclo–stationary process with period N. The signal power $P_m \triangleq \sum_{k=Nn}^{N(n+1)-1} \mathcal{E}\{|s_m[k]|^2\}$ per symbol interval at antenna m can be obtained as

$$\begin{aligned} P_m &= \sum_{i=-\infty}^{\infty} \sum_{j=-\infty}^{\infty} \sum_{k=Nn}^{N(n+1)-1} \varphi_{ff}^{m}[i-j]\tilde{g}_m[k-iN]\tilde{g}_m^*[k-jN] \\ &= \sum_{l=-\infty}^{\infty} \varphi_{ff}^{m}[l] \sum_{j=-\infty}^{\infty} \sum_{k=Nn}^{N(n+1)-1} \tilde{g}_m[k-jN-lN]\tilde{g}_m^*[k-jN] \\ &= \sum_{l=-\infty}^{\infty} \varphi_{ff}^{m}[l]\varphi_m[-Nl], \end{aligned} \tag{3.7}$$

where we define $\varphi_m[k]$ as

$$\varphi_m[k] \triangleq \tilde{g}_m[k] * \tilde{g}_m^*[-k]. \tag{3.8}$$

Now, P_m can be rewritten in vector form as $P_m = \boldsymbol{f}_m^H \boldsymbol{\Phi}_m \boldsymbol{f}_m$, and the total average transmit power constraint per symbol interval is then calculated as $P = \sum_{m=1}^{M} P_m$ and can be expressed as

$$P = \boldsymbol{f}^H \boldsymbol{\Phi} \boldsymbol{f} = 1 \tag{3.9}$$

with $ML_f \times ML_f$ block diagonal matrix $\boldsymbol{\Phi} \triangleq \mathrm{diag}\{\boldsymbol{\Phi}_1, \ldots, \boldsymbol{\Phi}_M\}$. Here, $\boldsymbol{\Phi}_m$ is a symmetric Toeplitz matrix as

$$\boldsymbol{\Phi}_m = \begin{bmatrix} \varphi_m[0] & \varphi_m[-N] & \ldots & \varphi_m[-N(L_f-1)] \\ \varphi_m[+N] & \varphi_m[0] & \ddots & \varphi_m[-N(L_f-2)] \\ \vdots & \vdots & \ddots & \vdots \\ \varphi_m[+N(L_f-1)] & \varphi_m[+N(L_f-2)] & \ldots & \varphi_m[0] \end{bmatrix}. \tag{3.10}$$

Combining Eqs. (3.5) and (3.9) we obtain the following Lagrange problem

$$L(\boldsymbol{f}, \alpha) = 1 + |\alpha|^2\sigma_c^2 - \alpha \boldsymbol{f}^H \boldsymbol{q} - \alpha^* \boldsymbol{q}^H \boldsymbol{f} + |\alpha|^2 \boldsymbol{f}^H \boldsymbol{Q}^H \boldsymbol{Q} \boldsymbol{f} + \lambda(\boldsymbol{f}^H \boldsymbol{\Phi} \boldsymbol{f} - 1), \tag{3.11}$$

where λ denotes the Lagrange multiplier. Differentiating $L(\boldsymbol{f}, \alpha)$ with respect to $\boldsymbol{f}^*$ and α^* we obtain

$$\frac{\partial L(\boldsymbol{f}, \alpha)}{\partial \boldsymbol{f}^*} = |\alpha|^2 \boldsymbol{Q}^H \boldsymbol{Q} \boldsymbol{f} - \alpha \boldsymbol{q} + \lambda \boldsymbol{\Phi} \boldsymbol{f} \tag{3.12}$$

and

$$\frac{\partial L(\boldsymbol{f}, \alpha)}{\partial \alpha^*} = \alpha \sigma_c^2 + \alpha \boldsymbol{f}^H \boldsymbol{Q}^H \boldsymbol{Q} \boldsymbol{f} - \boldsymbol{q}^H \boldsymbol{f}. \tag{3.13}$$

Setting the resulting gradients to zero leads to the optimum solution. To find the optimum solution faster we use an alternative formulation and define

$$\tilde{\boldsymbol{f}} = \alpha^* \boldsymbol{f}, \tag{3.14}$$

so the minimization criterion expressed in Eq. (3.5) can be rewritten as

$$\sigma_e^2 = 1 + |\alpha|^2 \sigma_c^2 - \tilde{\boldsymbol{f}}^H \boldsymbol{q} - \boldsymbol{q}^H \tilde{\boldsymbol{f}} + \tilde{\boldsymbol{f}}^H \boldsymbol{Q}^H \boldsymbol{Q} \tilde{\boldsymbol{f}}, \tag{3.15}$$

and the average transmit power constraint in Eq. (3.9) can be rewritten by multiplying both sides of the equation by $|\alpha|^2$ as

$$\tilde{\boldsymbol{f}}^H \boldsymbol{\Phi} \tilde{\boldsymbol{f}} = |\alpha|^2. \tag{3.16}$$

By substituting Eq. (3.16) in Eq. (3.15) we obtain

$$\sigma_e^2 = 1 + \tilde{\boldsymbol{f}}^H \boldsymbol{\Phi} \tilde{\boldsymbol{f}} \sigma_c^2 - \tilde{\boldsymbol{f}}^H \boldsymbol{q} - \boldsymbol{q}^H \tilde{\boldsymbol{f}} + \tilde{\boldsymbol{f}}^H \boldsymbol{Q}^H \boldsymbol{Q} \tilde{\boldsymbol{f}}. \tag{3.17}$$

Differentiating Eq. (3.17) with respect to $\tilde{\boldsymbol{f}}^*$ leads to

$$\frac{\partial \sigma_e^2}{\partial \tilde{\boldsymbol{f}}^*} = \left(\boldsymbol{Q}^H \boldsymbol{Q} + \sigma_c^2 \boldsymbol{\Phi} \right) \tilde{\boldsymbol{f}} - \boldsymbol{q}, \tag{3.18}$$

and setting the resulting gradient to zero, we calculate

$$\tilde{\boldsymbol{f}}_{\text{opt}} = \left(\boldsymbol{Q}^H \boldsymbol{Q} + \sigma_c^2 \boldsymbol{\Phi} \right)^{-1} \boldsymbol{q}. \tag{3.19}$$

Now, substituting Eq. (3.19) in Eqs. (3.14) and (3.16) leads to the optimum FIR solution as

$$\boldsymbol{f}_{\text{opt}} = \frac{1}{\alpha_{\text{opt}}^*} \left(\boldsymbol{Q}^H \boldsymbol{Q} + \sigma_c^2 \boldsymbol{\Phi} \right)^{-1} \boldsymbol{q} \tag{3.20}$$

$$\alpha_{\text{opt}} = \sqrt{\boldsymbol{q}^H \left(\boldsymbol{Q}^H \boldsymbol{Q} + \sigma_c^2 \boldsymbol{\Phi} \right)^{-1} \boldsymbol{\Phi} \left(\boldsymbol{Q}^H \boldsymbol{Q} + \sigma_c^2 \boldsymbol{\Phi} \right)^{-1} \boldsymbol{q}}. \tag{3.21}$$

As already mentioned in Section 2.3, α_{opt} is always positive and does not have to be implemented at the receiver.[1] Using Eqs. (3.20) and (3.21) in Eq. (3.5) we will have

$$\begin{aligned}\sigma^2_{e,\min} = 1 &+ \boldsymbol{q}^H \left(\boldsymbol{Q}^H\boldsymbol{Q} + \sigma_c^2\boldsymbol{\Phi}\right)^{-1} \left(\boldsymbol{Q}^H\boldsymbol{Q} + \sigma_c^2\boldsymbol{\Phi}\right) \left(\boldsymbol{Q}^H\boldsymbol{Q} + \sigma_c^2\boldsymbol{\Phi}\right)^{-1} \boldsymbol{q} \\ &- 2\boldsymbol{q}^H \left(\boldsymbol{Q}^H\boldsymbol{Q} + \sigma_c^2\boldsymbol{\Phi}\right) \boldsymbol{q}, \end{aligned} \tag{3.22}$$

which leads to the minimum error variance as

$$\sigma^2_{e,\min} = 1 - \boldsymbol{q}^H \left(\boldsymbol{Q}^H\boldsymbol{Q} + \sigma_c^2\boldsymbol{\Phi}\right)^{-1} \boldsymbol{q}. \tag{3.23}$$

For calculation of $\boldsymbol{f}_{\text{opt}}$ an $ML_f \times ML_f$ matrix has to be inverted, which is computationally expensive for large L_f. Therefore, from the complexity point of view short FIR filters are desirable. On the other hand, the performance of the proposed pre–equalization scheme improves with increasing L_f. Therefore, we are interested in finding the minimum value of L_f which achieves close–to–optimum performance. In this context, the optimum IIR solution is useful as it allows us to establish the ultimate performance limit of the proposed PEF scheme.

3.2 IIR Pre–Equalization Filters

As customary for IIR filter optimization, we drop the causality constraint and set $n_0 = 0$, and use a frequency–domain approach for filter optimization [33]. The frequency–domain approach simplifies our derivations as it avoids having to deal with infinite–length impulse responses. Furthermore, we denote the vector of IIR PEF frequency responses by $\boldsymbol{F}(e^{j\omega}) \triangleq [F_1(e^{j\omega}) \ldots F_M(e^{j\omega})]^H$, where $F_m(e^{j\omega}) \triangleq \mathcal{F}\{f_m[n]\}$. Similarly, the vector of the Fourier transforms of the sampled overall CIRs $q_m[Nn+k_0]$ is defined as $\boldsymbol{Q}(e^{j\omega}) \triangleq [Q_1(e^{j\omega}) \ldots Q_M(e^{j\omega})]^T$,

[1] We note that the error variance does not change if we multiply the right hand side of Eq. (3.21) with $e^{j\phi}$, where ϕ is an arbitrary phase. However, since from a practical point of view real–valued positive α_{opt} are desirable we concentrate on the case $\phi = 0$ in this thesis.

where $Q_m(e^{j\omega}) \triangleq \mathcal{F}\{q_m[Nn+k_0]\}$. Note that $Q_m(e^{j\omega})$ is related to the Fourier transform

$$\tilde{Q}_m(e^{j\omega}) \triangleq \mathcal{F}\{q_m[k+k_0]\} \tag{3.24}$$

of the overall CIR via [34]

$$Q_m(e^{j\omega}) = \frac{1}{N}\sum_{k=0}^{N-1} \tilde{Q}_m(e^{j(\omega-2\pi k)/N}). \tag{3.25}$$

For IIR PEFs without causality constraint (cf. Section 3.1) the definitions of $\boldsymbol{f}_m$, $\boldsymbol{q}_m$, and $\boldsymbol{Q}_m$ have to be slightly modified compared to the FIR case with causality constraint. For example, now $\boldsymbol{f}_m \triangleq [\ldots\ f_m[-1]\ f_m[0]\ f_m[1]\ \ldots]^T$ and $\boldsymbol{q}_m \triangleq [\ldots\ q_m[-N+k_0]\ q_m[k_0]\ q_m[N+k_0]\ \ldots]^T$ are valid. Taking these changes into account, $\boldsymbol{f}^H\boldsymbol{q}$ can be expressed as

$$\begin{aligned}
\boldsymbol{f}^H\boldsymbol{q} &= \sum_{m=1}^{M}\sum_{n=-\infty}^{\infty} f_m[n]q_m[-Nn+k_0] \\
&= \frac{1}{2\pi}\sum_{m=1}^{M}\sum_{n=-\infty}^{\infty}\int_{-\pi}^{\pi} F_m(e^{j\omega})q_m[-Nn+k_0]e^{j\omega n}\,\mathrm{d}\omega \\
&= \frac{1}{2\pi}\int_{-\pi}^{\pi}\sum_{m=1}^{M} F_m(e^{j\omega})Q_m(e^{j\omega})\,\mathrm{d}\omega \\
&= \frac{1}{2\pi}\int_{-\pi}^{\pi} \boldsymbol{F}^H(e^{j\omega})\boldsymbol{Q}(e^{j\omega})\,\mathrm{d}\omega,
\end{aligned} \tag{3.26}$$

where we have used the definition of the (inverse) discrete–time Fourier transform. Taking the non–causality and IIR property into account in the definition of $\boldsymbol{Q}_m$, $\boldsymbol{f}^H\boldsymbol{Q}^H\boldsymbol{Q}\boldsymbol{f}$ can be rewritten as

$$\begin{aligned}
\boldsymbol{f}^H\boldsymbol{Q}^H\boldsymbol{Q}\boldsymbol{f} &= \sum_{m=1}^{M} ||\boldsymbol{Q}_m\boldsymbol{f}_m||^2 \\
&= \sum_{m=1}^{M}\sum_{n=-\infty}^{\infty} |x_m[n]|^2 = \frac{1}{2\pi}\int_{-\pi}^{\pi}\sum_{m=1}^{M} |X_m(e^{j\omega})|^2\,\mathrm{d}\omega \\
&= \frac{1}{2\pi}\int_{-\pi}^{\pi} \boldsymbol{F}^H(e^{j\omega})\boldsymbol{Q}(e^{j\omega})\boldsymbol{Q}^H(e^{j\omega})\boldsymbol{F}(e^{j\omega})\,\mathrm{d}\omega,
\end{aligned} \tag{3.27}$$

where we have employed the definitions $x_m[n] \triangleq f_m[n] * q_m[Nn + k_0]$ and $X_m(e^{j\omega}) \triangleq \mathcal{F}\{x_m[n]\} = F_m(e^{j\omega})Q_m(e^{j\omega})$, and Parseval's theorem [34]

$$\sum_{n=-\infty}^{\infty} |x[n]|^2 = \frac{1}{2\pi} \int_{-\pi}^{\pi} |X(\omega)|^2 d\omega. \tag{3.28}$$

Applying Eqs. (3.26) and (3.27) in Eq. (3.5) the error variance can be rewritten as

$$\sigma_e^2 = 1 + |\alpha|^2\sigma_c^2 - \frac{1}{2\pi} \int_{-\pi}^{\pi} \left[\alpha \boldsymbol{F}^H(e^{j\omega})\boldsymbol{Q}(e^{j\omega}) + \alpha^* \boldsymbol{Q}^H(e^{j\omega})\boldsymbol{F}(e^{j\omega})\right] \mathrm{d}\omega$$
$$+ \frac{1}{2\pi} \int_{-\pi}^{\pi} |\alpha|^2 \boldsymbol{F}^H(e^{j\omega})\boldsymbol{Q}(e^{j\omega})\boldsymbol{Q}^H(e^{j\omega})\boldsymbol{F}(e^{j\omega}) \,\mathrm{d}\omega. \tag{3.29}$$

Similarly, using the definitions

$$\boldsymbol{\Phi}(e^{j\omega}) \triangleq \mathrm{diag}\{\Phi_1(e^{j\omega}),\, \Phi_2(e^{j\omega}),\, \ldots,\, \Phi_M(e^{j\omega})\}, \tag{3.30}$$

and

$$\Phi_m(e^{j\omega}) \triangleq \mathcal{F}\{\varphi_m[Nn]\}, \tag{3.31}$$

and based on Eq.(3.7) we may rewrite the signal power for antenna m as

$$P_m = \frac{1}{2\pi} \sum_{l=-\infty}^{\infty} \int_{-\pi}^{\pi} \Phi_{ff}^m(e^{j\omega})\varphi_m[-Nl]e^{j\omega l} \,\mathrm{d}\omega = \frac{1}{2\pi} \int_{-\pi}^{\pi} |F_m(e^{j\omega})|^2 \Phi_m(e^{j\omega}) \,\mathrm{d}\omega, \tag{3.32}$$

where we have used the definition of the (inverse) Fourier transform and the identity $\Phi_{ff}^m(e^{j\omega}) \triangleq \mathcal{F}\{\varphi_{ff}^m[k]\} = |F_m(e^{j\omega})|^2$. By adding the powers P_m, $1 \leq m \leq M$, of all M antennas we obtain the average transmit power constraint as

$$P = \frac{1}{2\pi} \int_{-\pi}^{\pi} \boldsymbol{F}^H(e^{j\omega})\boldsymbol{\Phi}(e^{j\omega})\boldsymbol{F}(e^{j\omega}) \,\mathrm{d}\omega = 1. \tag{3.33}$$

We note that the Fourier transform $\Phi_m(e^{j\omega})$ of the sampled sequence $\varphi_m[Nn]$ is related to the Fourier transform

$$\tilde{\Phi}_m(e^{j\omega}) \triangleq \mathcal{F}\{\varphi_m[k]\} \tag{3.34}$$

of the sequence by [34]

$$\Phi_m(e^{j\omega}) = \frac{1}{N}\sum_{k=0}^{N-1}\tilde{\Phi}_m(e^{j(\omega-2\pi k)/N}). \tag{3.35}$$

Based on Eqs. (3.29) and (3.33) we can formulate a Lagrange problem similar to Eq. (3.11) in the FIR case. Again, as an alternative formulation we define

$$\tilde{\boldsymbol{F}}(e^{i\omega}) = \alpha^*\boldsymbol{F}(e^{i\omega}), \tag{3.36}$$

therefore the average transmit power constraint in Eq. (3.33) can be rewritten as

$$|\alpha|^2 = \frac{1}{2\pi}\int_{-\pi}^{\pi}\tilde{\boldsymbol{F}}^H(e^{i\omega})\boldsymbol{\Phi}(e^{j\omega})\tilde{\boldsymbol{F}}(e^{i\omega})\,\mathrm{d}\omega. \tag{3.37}$$

From this, we find the error variance as

$$\begin{aligned}\sigma_e^2 = 1 &- \frac{1}{2\pi}\int_{-\pi}^{\pi}\tilde{\boldsymbol{F}}^H(e^{i\omega})\boldsymbol{Q}(e^{i\omega})\,\mathrm{d}\omega - \frac{1}{2\pi}\int_{-\pi}^{\pi}\boldsymbol{Q}^H(e^{i\omega})\tilde{\boldsymbol{F}}(e^{i\omega})\,\mathrm{d}\omega \\ &+ \frac{\sigma_c^2}{2\pi}\int_{-\pi}^{\pi}\tilde{\boldsymbol{F}}^H(e^{i\omega})\boldsymbol{\Phi}(e^{j\omega})\tilde{\boldsymbol{F}}(e^{i\omega})\,\mathrm{d}\omega + \frac{1}{2\pi}\int_{-\pi}^{\pi}\tilde{\boldsymbol{F}}^H(e^{i\omega})\boldsymbol{Q}(e^{j\omega})\boldsymbol{Q}^H(e^{j\omega})\tilde{\boldsymbol{F}}(e^{i\omega})\,\mathrm{d}\omega.\end{aligned} \tag{3.38}$$

To solve this problem we differentiate Eq. (3.38) with respect to $\tilde{\boldsymbol{F}}^*(e^{i\omega})$ and find

$$\frac{\partial\sigma_e^2}{\partial\tilde{\boldsymbol{F}}^*(e^{i\omega})} = \sigma_c^2\boldsymbol{\Phi}(e^{i\omega})\tilde{\boldsymbol{F}}(e^{i\omega}) + \boldsymbol{Q}(e^{i\omega})\boldsymbol{Q}^H(e^{i\omega})\tilde{\boldsymbol{F}}(e^{i\omega}) - \boldsymbol{Q}(e^{i\omega}). \tag{3.39}$$

Setting the resulting gradient to zero, we calculate

$$\tilde{\boldsymbol{F}}(e^{i\omega}) = \left(\boldsymbol{Q}(e^{i\omega})\boldsymbol{Q}^H(e^{i\omega}) + \sigma_c^2\boldsymbol{\Phi}(e^{i\omega})\right)^{-1}\boldsymbol{Q}(e^{i\omega}). \tag{3.40}$$

Finally, substituting Eq. (3.40) in Eqs. (3.36) and (3.37) leads to the optimum IIR PEFs

$$\boldsymbol{F}_{\mathrm{opt}}(e^{j\omega}) = \frac{1}{\alpha_{\mathrm{opt}}^*}\boldsymbol{M}(e^{j\omega})\boldsymbol{Q}(e^{j\omega}) \tag{3.41}$$

$$\alpha_{\mathrm{opt}} = \sqrt{\frac{1}{2\pi}\int_{-\pi}^{\pi}\boldsymbol{Q}^H(e^{j\omega})\boldsymbol{M}(e^{j\omega})\boldsymbol{\Phi}(e^{j\omega})\boldsymbol{M}(e^{j\omega})\boldsymbol{Q}(e^{j\omega})\,\mathrm{d}\omega}, \tag{3.42}$$

with $\boldsymbol{M}(e^{j\omega}) \triangleq (\boldsymbol{Q}(e^{j\omega})\boldsymbol{Q}^H(e^{j\omega}) + \sigma_c^2\boldsymbol{\Phi}(e^{j\omega}))^{-1}$. Using the matrix inversion lemma [35], we obtain

$$\boldsymbol{M}(e^{j\omega}) = \frac{\boldsymbol{\Phi}^{-1}(e^{j\omega})}{\sigma_c^2}\left[\boldsymbol{I}_M - \frac{\boldsymbol{Q}(e^{j\omega})\boldsymbol{Q}^H(e^{j\omega})\boldsymbol{\Phi}^{-1}(e^{j\omega})}{\sigma_c^2 + \boldsymbol{Q}^H(e^{j\omega})\boldsymbol{\Phi}^{-1}(e^{j\omega})\boldsymbol{Q}(e^{j\omega})}\right]. \tag{3.43}$$

With this result Eqs. (3.41) and (3.42) can be simplified to

$$F_m^{\text{opt}}(e^{j\omega}) = \frac{1}{\alpha_{\text{opt}}^*}\frac{Q_m(e^{j\omega})}{\Phi_m(e^{j\omega})(\sigma_c^2 + X(e^{j\omega}))} \tag{3.44}$$

$$\alpha_{\text{opt}} = \sqrt{\frac{1}{2\pi}\int_{-\pi}^{\pi}\frac{X(e^{j\omega})}{(\sigma_c^2 + X(e^{j\omega}))^2}\,\mathrm{d}\omega}, \tag{3.45}$$

where

$$\begin{aligned} X(e^{j\omega}) &= \boldsymbol{Q}^H(e^{j\omega})\boldsymbol{\Phi}^{-1}(e^{j\omega})\boldsymbol{Q}(e^{j\omega}) \\ &= \sum_{m=1}^{M}\frac{|Q_m(e^{j\omega})|^2}{\Phi_m(e^{j\omega})}, \end{aligned} \tag{3.46}$$

and $F_m^{\text{opt}}(e^{j\omega})$, $1 \le m \le M$, denotes the mth component of $\boldsymbol{F}_{\text{opt}}(e^{j\omega})$. The corresponding minimum error variance can be obtained from Eqs. (3.29) and (3.46) as

$$\sigma_{e,\min}^2 = \frac{1}{2\pi}\int_{-\pi}^{\pi}\frac{\sigma_c^2}{\sigma_c^2 + X(e^{j\omega})}\,\mathrm{d}\omega. \tag{3.47}$$

3.3 Performance Analysis

In this section, we provide an expression for the BER of the proposed pre–equalization scheme. For this purpose we assume that the residual ISI is approximately Gaussian distributed, which is typically a good assumption for MMSE problems [36]. For this purpose, we first assume that FIR PEFs are used and note that the receiver output signal can be expressed as

$$r[n] = \boldsymbol{f}^H\boldsymbol{q}a[n-n_0] + \boldsymbol{f}^H\boldsymbol{Q}^H\boldsymbol{a}_{n_0}[n] + z_s[n], \tag{3.48}$$

where $\boldsymbol{a}_{n_0}[n]$ is identical to $\boldsymbol{a}[n]$ except that its n_0th component is zero. Based on this representation, it can be observed that the effective SNR of the decision

variable $r[n]$ can be easily calculated. The first term in Eq. (3.48) represents the signal contribution, whereas the second and third term represent the residual interference contribution and the noise, respectively. Therefore, the signal power γ can be found as

$$\gamma = \left| \boldsymbol{f}^H \boldsymbol{q} \right|^2, \tag{3.49}$$

and the effective variance of residual ISI and noise, denoted as σ^2, can be expressed as

$$\begin{aligned} \sigma^2 &= (\boldsymbol{Q}\boldsymbol{f})^H \, \tilde{\boldsymbol{I}}_{n_0} \, (\boldsymbol{Q}\boldsymbol{f}) + \sigma_s^2 \\ &= \boldsymbol{f}^H \boldsymbol{Q}^H \boldsymbol{Q} \boldsymbol{f} - \left| \boldsymbol{f}^H \boldsymbol{q} \right|^2 + \sigma_c^2, \end{aligned} \tag{3.50}$$

where $\tilde{\boldsymbol{I}}_{n_0}$ is the identity matrix except that its n_0th diagonal component is zero instead of one. Note that $\sigma_s^2 \triangleq \mathcal{E}\{|z_s[n]|^2\} = \sigma_c^2$ as shown in Section (2.3). Now the effective SNR of the decision variable $r[n]$ can be calculated as

$$\text{SNR} = \frac{|\boldsymbol{f}^H \boldsymbol{q}|^2}{\boldsymbol{f}^H \boldsymbol{Q}^H \boldsymbol{Q} \boldsymbol{f} - |\boldsymbol{f}^H \boldsymbol{q}|^2 + \sigma_c^2}. \tag{3.51}$$

By replacing Eqs. (3.20), (3.21), and (3.23) in Eq. (3.51) we obtain

$$\begin{aligned} \text{SNR} &= \frac{\boldsymbol{q}^H (\boldsymbol{Q}^H \boldsymbol{Q} + \sigma_c^2 \boldsymbol{\Phi})^{-1} \boldsymbol{q}}{1 - \boldsymbol{q}^H (\boldsymbol{Q}^H \boldsymbol{Q} + \sigma_c^2 \boldsymbol{\Phi})^{-1} \boldsymbol{q}} \\ &= \frac{1}{\sigma_{e,\min}^2} - 1. \end{aligned} \tag{3.52}$$

Assuming now that the residual interference term $\boldsymbol{f}^H \boldsymbol{Q}^H \boldsymbol{a}_{n_0}[n] + z_s[n]$ is approximately Gaussian distributed, we obtain for the BER of the proposed FIR pre–equalization scheme the expression

$$P_e = Q\left(\sqrt{2 \left(\frac{1}{\sigma_{e,\min}^2} - 1 \right)} \right). \tag{3.53}$$

The same expression is also valid for IIR PEFs if the corresponding error variance $\sigma_{e,\min}^2$ given in Eq. (3.47) is used.

3.4 Optimality of A–Pre–Rake for IIR PEFs

It is well known that the performance of pre–Rake (and post–Rake) receivers does not necessarily improve if the number of Rake fingers is increased, cf. e.g. [37]. When there is significant ISI in the system, a carefully chosen number of Rake fingers of an S–pre–Rake filter can achieve better performance than the A–pre–Rake filter. The reason for this behavior is that while more energy can be collected by increasing the number of fingers, the amount of residual ISI may also increase. A similar effect can also be observed if the pre–Rake filters are enhanced with short FIR PEFs. However, we will show in the following that the A–pre–Rake filter is indeed optimum if the PEFs are sufficiently long. For this purpose we rewrite $X(e^{j\omega})$. Using Eq. (3.8) in Eq. (3.34) we obtain

$$\tilde{\Phi}_m(e^{j\omega}) = |\tilde{G}_m(e^{j\omega})|^2, \tag{3.54}$$

where $\tilde{G}_m(e^{j\omega}) \triangleq \mathcal{F}\{\tilde{g}_m[k]\}$. Now, based on Eq. (3.35) we find

$$\Phi_m(e^{j\omega}) = \frac{1}{N}\sum_{k=0}^{N-1} |\tilde{G}_m(e^{j(\omega-2\pi k)/N})|^2. \tag{3.55}$$

Using Eq. (6.8) in Eq. (3.24) we obtain

$$\tilde{Q}_m(e^{j\omega}) = e^{j\omega k_0}\tilde{G}_m(e^{j\omega})\tilde{H}_m(e^{j\omega}), \tag{3.56}$$

where $\tilde{H}_m(e^{j\omega}) \triangleq \mathcal{F}\{\tilde{h}_m[k]\}$, and based on Eq. (3.25) we find

$$|Q_m(e^{j\omega})|^2 = \frac{1}{N}|\sum_{k=0}^{N-1} \tilde{G}_m(e^{j(\omega-2\pi k)/N})e^{j(\omega-2\pi k)k_0/N}\tilde{H}_m(e^{j(\omega-2\pi k)/N})|^2. \tag{3.57}$$

Now replacing Eq. (3.55) and (3.57) in Eq. (3.46) we can rewrite $X(e^{j\omega})$ as

$$X(e^{j\omega}) = \frac{1}{N}\sum_{m=1}^{M} \frac{|\sum_{k=0}^{N-1} \tilde{G}_m(e^{j(\omega-2\pi k)/N})e^{j(\omega-2\pi k)k_0/N}\tilde{H}_m(e^{j(\omega-2\pi k)/N})|^2}{\sum_{k=0}^{N-1}|\tilde{G}_m(e^{j(\omega-2\pi k)/N})|^2}. \tag{3.58}$$

Using the Cauchy–Schwarz inequality [35] it can be shown that $X(e^{j\omega})$ is maximized if $\tilde{G}_m(e^{j\omega}) = e^{-j\omega k_0}\tilde{H}_m^*(e^{j\omega})$ corresponding to an A–pre–Rake (or

time–reversal) filter for each branch m, $1 \leq m \leq M$. Therefore, the A–pre–Rake filter minimizes the error variance $\sigma^2_{e,\min}$ and is thus optimum if IIR PEFs are employed. In this case, the corresponding minimum error variance in Eq. (3.47) is given by

$$\sigma^2_{e,\min} = \frac{1}{2\pi} \int_{-\pi}^{\pi} \frac{\sigma_c^2}{\sigma_c^2 + \frac{1}{N} \sum_{m=1}^{M} \sum_{k=0}^{N-1} |\tilde{H}_m(e^{j(\omega - 2\pi k)/N})|^2} \, \mathrm{d}\omega. \tag{3.59}$$

Increasing the spreading factor N improves performance by decreasing the effective spectral fluctuation for a given m, i.e., $\frac{1}{N} \sum_{k=0}^{N-1} |\tilde{H}_m(e^{j(\omega - 2\pi k)/N})|^2$ becomes smoother which has a positive effect on $\sigma^2_{e,\min}$ in Eq. (3.59). Increasing the number of antennas has a similar effect, but also provides an additional combining gain. The impact of N on the performance of the proposed PEF scheme will be investigated more in detail in Section 3.6.

3.5 Performance Bound

A meaningful performance bound for any (pre–)equalizer and any (pre–)Rake scheme is the so–called matched–filter (MF) bound [38]. For the MF bound we assume that the optimum A–pre–Rake filter is used at the transmitter and ignore any interference caused at the receiver. The resulting SNR is

$$\mathrm{SNR}_{\mathrm{MF}} = \frac{1}{\sigma_c^2} \sum_{m=1}^{M} \sum_{k=-\infty}^{\infty} |\tilde{h}_m[k]|^2 = \frac{1}{2\pi\sigma_c^2} \sum_{m=1}^{M} \int_{-\pi}^{\pi} |\tilde{H}_m(e^{j\omega})|^2 \, \mathrm{d}\omega, \tag{3.60}$$

where we have applied Parseval's theorem [34]. The corresponding BER lower bound is

$$P_{\mathrm{MF}} = Q\left(\sqrt{2\mathrm{SNR}_{\mathrm{MF}}}\right), \tag{3.61}$$

i.e., no implementable (pre–)equalizer and (pre–)Rake scheme will achieve a better performance.

3.6 Performance for Large Spreading Factors

It is interesting to investigate the performance of the proposed PEF scheme for the case of long spreading sequences, i.e., $N \to \infty$. For $N \to \infty$ the summations over $0 \leq k < N$ in Eq. (3.58) can be replaced by integrals and $X(e^{j\omega}) = X$ becomes independent of ω.

In particular, we obtain

$$X = \sum_{m=1}^{M} \frac{\left| \frac{1}{2\pi} \int_{-\pi}^{\pi} \tilde{G}_m(e^{j\omega}) e^{j\omega k_0} \tilde{H}_m(e^{j\omega}) \, \mathrm{d}\omega \right|^2}{\frac{1}{2\pi} \int_{-\pi}^{\pi} |\tilde{G}_m(e^{j\omega})|^2 \, \mathrm{d}\omega}, \tag{3.62}$$

and with Eqs. (3.47) and (3.52) the resulting effective SNR is

$$\mathrm{SNR} = X/\sigma_c^2. \tag{3.63}$$

For the special case of an A–pre–Rake filter X simplifies to

$$X = \frac{1}{2\pi} \sum_{m=1}^{M} \int_{-\pi}^{\pi} |\tilde{H}_m(e^{j\omega})|^2 \, \mathrm{d}\omega, \tag{3.64}$$

i.e., and the SNR becomes

$$\mathrm{SNR} = \frac{1}{2\pi\sigma_c^2} \sum_{m=1}^{M} \int_{-\pi}^{\pi} |\tilde{H}_m(e^{j\omega})|^2 \, \mathrm{d}\omega = \mathrm{SNR}_{\mathrm{MF}}. \tag{3.65}$$

Consequently, the proposed transmitter structure approaches the MF bound performance limit for sufficiently long spreading sequences. This result is intuitively pleasing since $N \to \infty$ means that the overall CIR, $q[Nn]$ is ISI–free, and linear processing at the transmitter is optimum.

Chapter 4

Uplink–Downlink Duality

In this chapter, we study a SIMO DS–UWB system with M receive antennas, post–Rake combining, and post–equalization, cf. Fig. 4.1. We will also refer to the SIMO system in Fig. 4.1 as the *uplink* to distinguish it from the MISO downlink configuration shown in Fig. 2.1. For $\tilde{h}_m[k]$ and $\tilde{g}_m[k]$ in Fig. 4.1 the

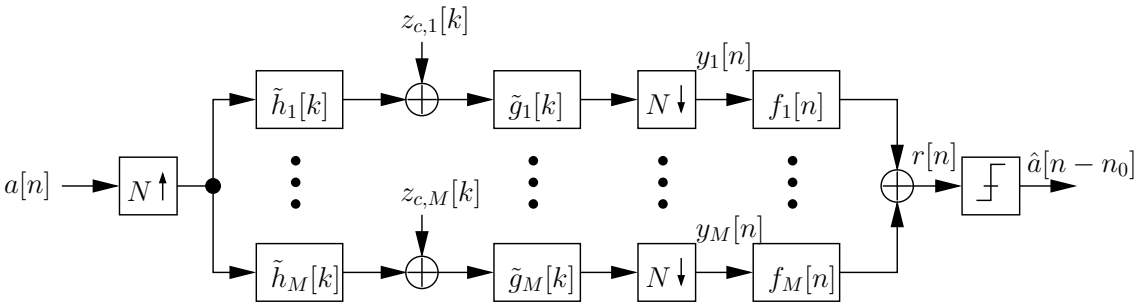

Figure 4.1: Block diagram of a SIMO DS–UWB system (uplink) with M receive antennas, post–Rake combining, and post–equalization.

definitions provided in Section 2 are still valid, i.e., $\tilde{h}_m[k]$ contains the combined effects of spreading with $c[N-1-k]$ and the CIR of antenna m, whereas $\tilde{g}_m[k]$ contains the combined effects of de–spreading with $c[k]$ and post–Rake combining. Each receive antenna employs a post–equalization filter $f_m[n]$, $1 \leq m \leq M$, to remove residual ISI before a decision is made. The noise processes $z_{c,m}[k]$, $1 \leq m \leq M$, are mutually independent AWGN processes

with variance σ_c^2.

We derive the optimum filter coefficients for the *uplink* structure in Section 4.1, and show its relationship to that of the *downlink* structure, followed by a brief discussion on practical implications of the uplink–downlink duality in Section 4.2.

4.1 Filter Optimization

In the following, we assume FIR filters $f_m[n]$, $1 \leq m \leq M$, and optimize them based on the MMSE criterion. We note that for $\boldsymbol{Q}$, $\boldsymbol{q}$, $\boldsymbol{\Phi}$, and $\boldsymbol{f}$ the same definitions as for the MISO downlink problem considered in Section 3.1 are valid. The received signal $r[n]$ in Fig. 4.1 can be expressed as

$$\begin{aligned} r[n] &= \sum_{m=1}^{M} (\boldsymbol{Q}_m \boldsymbol{f}_m)^H \boldsymbol{a}[n] + \sum_{m=1}^{M} \boldsymbol{f}_m^H z_m[n] \\ &= (\boldsymbol{Q}\boldsymbol{f})^H \boldsymbol{a}[n] + \boldsymbol{f}^H \boldsymbol{z}[n], \end{aligned} \tag{4.1}$$

where $\boldsymbol{z}[n] \triangleq [\boldsymbol{z}_1^T[n] \ \ldots \ \boldsymbol{z}_M^T[n]]^T$, $\boldsymbol{z}_m[n] \triangleq [z_m[n] \ z_m[n-1] \ \ldots \ z_m[n-L_f+1]]^T$, and

$$z_m[n] = \sum_{l=-\infty}^{\infty} z_{c,m}[l] \tilde{g}_m[Nn - l]. \tag{4.2}$$

Based on Eq. (4.2) the autocorrelation function of $z_m[n]$ can be calculated as

$$\begin{aligned} \varphi_{zz}^m[n] &= \mathcal{E}\{z_m[\lambda + n] z_m^*[\lambda]\} \\ &= \sum_{l=1}^{M} \sum_{k=1}^{M} \tilde{g}_m[l] \tilde{g}_m^*[k] \mathcal{E}\left\{z_{c,m}[N(\lambda + n) - l] z_{c,m}^*[N\lambda - k]\right\} \\ &= \sum_{l=1}^{M} \sum_{k=1}^{M} \tilde{g}_m[l] \tilde{g}_m^*[k] \sigma_c^2 \delta[Nn + k - l] \\ &= \sigma_c^2 \sum_{l=1}^{M} \sum_{k=1}^{M} \tilde{g}_m[N(\lambda + n) - l] \tilde{g}_m^*[N\lambda - k] \delta[l - k] \\ &= \sigma_c^2 \sum_{l=1}^{M} \tilde{g}_m[Nn - l] \tilde{g}_m^*[-l] \end{aligned}$$

$$= \sigma_c^2 \varphi_m[Nn], \tag{4.3}$$

with $\varphi_m[k]$ as defined in Section 3.1. Exploiting this result we can express the error variance to be minimized as

$$\begin{aligned}\sigma_e^2 &\triangleq \mathcal{E}\{|a[n-n_0] - r[n]|^2\} \\ &= 1 - \mathcal{E}\left\{a^*[n-n_0]r[n]\right\} - \mathcal{E}\left\{a[n-n_0]r^*[n]\right\} + \mathcal{E}\left\{|r[n]|^2\right\}, \end{aligned} \tag{4.4}$$

and replacing $r[n]$ from Eq. (4.1) in Eq. (4.4) will lead to

$$\sigma_e^2 = 1 - \sum_{m=1}^{M} \boldsymbol{q}_m^H \boldsymbol{f}_m - \sum_{m=1}^{M} \boldsymbol{f}_m^H \boldsymbol{q}_m + \boldsymbol{f}^H \boldsymbol{Q}^H \boldsymbol{Q} \boldsymbol{f} + \boldsymbol{f}^H \boldsymbol{\Phi}_z \boldsymbol{f}. \tag{4.5}$$

Note that $\boldsymbol{\Phi}_z = \mathcal{E}\left\{\boldsymbol{z}\boldsymbol{z}^H\right\} = \text{diag}\{\boldsymbol{\Phi}_z^1, \ldots, \boldsymbol{\Phi}_z^M\}$, where $\boldsymbol{\Phi}_z^m = \mathcal{E}\left\{\boldsymbol{z}_m \boldsymbol{z}_m^H\right\} = \sigma_c^2 \boldsymbol{\Phi}_m$, and therefore $\boldsymbol{\Phi}_z^m = \sigma_c^2 \boldsymbol{\Phi}$. Replacing $\boldsymbol{\Phi}_z$ in Eq. (4.5) we obtain

$$\begin{aligned}\sigma_e^2 &= 1 - \boldsymbol{f}^H \boldsymbol{q} - \boldsymbol{q}^H \boldsymbol{f} + \boldsymbol{f}^H \boldsymbol{Q}^H \boldsymbol{Q} \boldsymbol{f} + \sigma_c^2 \boldsymbol{f}^H \boldsymbol{\Phi} \boldsymbol{f} \\ &= 1 - \boldsymbol{f}^H \boldsymbol{q} - \boldsymbol{q}^H \boldsymbol{f} + \boldsymbol{f}^H \left(\boldsymbol{Q}^H \boldsymbol{Q} + \sigma_c^2 \boldsymbol{\Phi}\right) \boldsymbol{f}. \end{aligned} \tag{4.6}$$

To minimize σ_e^2, we differentiate it with respect to $\boldsymbol{f}^*$ which leads to

$$\frac{\partial \sigma_e^2}{\partial \tilde{\boldsymbol{f}}^*} = \left(\boldsymbol{Q}^H \boldsymbol{Q} + \sigma_c^2 \boldsymbol{\Phi}\right) \boldsymbol{f} - \boldsymbol{q}. \tag{4.7}$$

Setting the resulting gradient to zero, we obtain the optimum vector

$$\boldsymbol{f}_{\text{opt}}^{\text{uplink}} = (\boldsymbol{Q}^H \boldsymbol{Q} + \sigma_c^2 \boldsymbol{\Phi})^{-1} \boldsymbol{q}. \tag{4.8}$$

By replacing $\boldsymbol{f}_{\text{opt}}^{\text{uplink}}$ in Eq. (4.6) the minimum error variance will be obtained identical to $\sigma_{e,\min}^2$ given in Eq. (3.23) for the *downlink*, according to

$$\sigma_{e,\min}^2 = 1 - \boldsymbol{q}^H \left(\boldsymbol{Q}^H \boldsymbol{Q} + \sigma_c^2 \boldsymbol{\Phi}\right)^{-1} \boldsymbol{q}. \tag{4.9}$$

This means the optimum SIMO uplink post–equalization filters in Eq. (4.8) are up to an irrelevant scaling factor identical to the optimum MISO downlink PEFs. Furthermore, it can easily be verified that the minimum error variances are identical in both cases. In other words, there is a duality between SIMO MMSE post–equalization after post–Rake combining and MISO MMSE pre–equalization before pre–Rake combining. We note that this duality also holds if IIR MMSE equalization filters are employed, of course.

4.2 Practical Implications

The uplink–downlink duality of the above MMSE problem is not only of theoretical interest but also has important practical implications. In particular, while adaptive algorithms cannot be used to calculate the optimum downlink filter $\boldsymbol{f}_{\text{opt}}$ since the received signal $r[n]$ is not available at the transmitter, the uplink filter $\boldsymbol{f}_{\text{opt}}^{\text{uplink}}$ can be efficiently calculated using an adaptive algorithm such as the least–mean square (LMS) or the recursive least squares (RLS) algorithm [39]. For example, with the LMS algorithm the uplink filters are updated according to

$$\boldsymbol{f}_{\text{uplink}}[n+1] = \boldsymbol{f}_{\text{uplink}}[n] + \mu_0 e^*[n]\boldsymbol{y}[n], \tag{4.10}$$

where μ_0 and $e[n] \triangleq a[n-n_0] - r[n]$ denote the adaptation step size and the error signal, respectively. Furthermore, $\boldsymbol{y}[n] \triangleq [\boldsymbol{y}_1^T[n] \ \ldots \ \boldsymbol{y}_M^T[n]]^T$, $\boldsymbol{y}_m[n] \triangleq [y_m[n] \ y_m[n-1] \ \ldots \ y_m[n-L_f+1]]^T$, and $y_m[n]$ denotes the input signal for the equalization filter at antenna m, $1 \leq m \leq M$, cf. Fig. 4.1. We note that for calculation of the error signal, $a[n-n_0]$ can either be a training symbol or a previously decided symbol. Once the LMS has converged and $\boldsymbol{f}_{\text{opt}}^{\text{uplink}}$ is known, the normalization factor α required in the downlink can be obtained from

$$\alpha_{\text{opt}} = \sqrt{(\boldsymbol{f}_{\text{opt}}^{\text{uplink}})^H \boldsymbol{\Phi} \boldsymbol{f}_{\text{opt}}^{\text{uplink}}}, \tag{4.11}$$

and the optimum downlink PEF is

$$\boldsymbol{f}_{\text{opt}} = \frac{\boldsymbol{f}_{\text{opt}}^{\text{uplink}}}{\alpha_{\text{opt}}}. \tag{4.12}$$

It should be noted that $\boldsymbol{\Phi}$ only depends on the pre–Rake filter coefficients. Therefore, the proposed recursive calculation of the optimum MISO downlink PEF $\boldsymbol{f}_{\text{opt}}$ only requires knowledge of the pre–Rake filter coefficients. For the P- and S–pre–Rake filter estimation of the entire CIRs, $h_m[k]$, $0 \leq k < L_h$, $1 \leq m \leq M$, which is necessary for the closed–form solution in Eq. (3.20), can thus be avoided.

Chapter 5

Simplified PEF Structure

In this chapter, we consider the simplified PEF (S–PEF) structure for the MISO downlink shown in Fig. 5.1. The main difference to the PEF structure shown in Fig. 2.1 is that only one PEF $\boldsymbol{f} \triangleq [f[0] \ \ldots \ f[L_f - 1]]^T$ is employed jointly for all $M > 1$ transmit antennas, which reduces transmitter complexity.

In the next section we derive the optimum FIR S–PEF coefficients and pro-

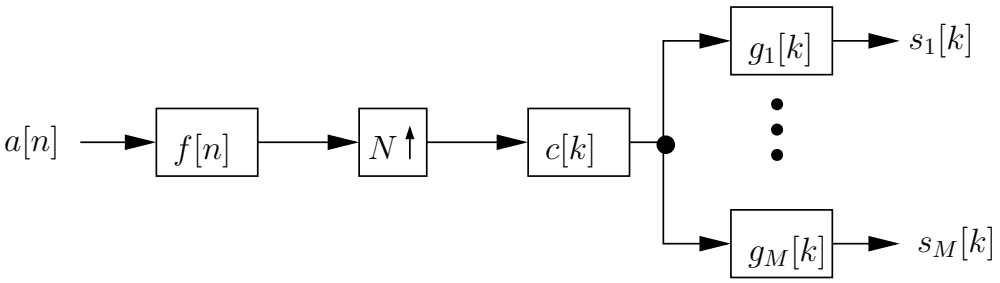

Figure 5.1: Block diagram of a MISO DS–UWB system (downlink) with M transmit antennas, pre–Rake combining, and simplified pre–equalization.

vide an expression for the corresponding minimum error variance. The IIR filter optimization follow in Section 5.2 and expressions for the corresponding minimum error variance and the approximate BER of the S–PEF scheme for the IIR case are provided.

5.1 FIR Filter Optimization

As far as filter optimization is concerned, the S–PEF structure shown in Fig. 5.1 leads to an equivalent single–input single–output (SISO) channel with effective overall CIR

$$q_{\text{eff}}[Nn + k_0] = \sum_{m=1}^{M} q_m[Nn + k_0], \tag{5.1}$$

and transmit power

$$P = \boldsymbol{f}^H \boldsymbol{\Phi}_{\text{eff}} \boldsymbol{f}, \tag{5.2}$$

where

$$\boldsymbol{\Phi}_{\text{eff}} = \sum_{m=1}^{M} \boldsymbol{\Phi}_m. \tag{5.3}$$

Consequently, based on the results in Section 3.1 the optimum FIR PEF is obtained by replacing $\boldsymbol{q}$, $\boldsymbol{Q}$, and $\boldsymbol{\Phi}$ in Eqs. (3.20) and (3.21) by $\boldsymbol{q}_{\text{eff}}$, $\boldsymbol{Q}_{\text{eff}}$, and $\boldsymbol{\Phi}_{\text{eff}}$, respectively, and is thus given by

$$\boldsymbol{f}_{\text{opt}} = \frac{1}{\alpha^*_{\text{opt}}} \left(\boldsymbol{Q}^H_{\text{eff}} \boldsymbol{Q}_{\text{eff}} + \sigma_c^2 \boldsymbol{\Phi}_{\text{eff}} \right)^{-1} \boldsymbol{q}_{\text{eff}} \tag{5.4}$$

$$\alpha_{\text{opt}} = \sqrt{\boldsymbol{q}^H_{\text{eff}} \left(\boldsymbol{Q}^H_{\text{eff}} \boldsymbol{Q}_{\text{eff}} + \sigma_c^2 \boldsymbol{\Phi}_{\text{eff}} \right)^{-1} \boldsymbol{\Phi}_{\text{eff}} \left(\boldsymbol{Q}^H_{\text{eff}} \boldsymbol{Q}_{\text{eff}} + \sigma_c^2 \boldsymbol{\Phi}_{\text{eff}} \right)^{-1} \boldsymbol{q}_{\text{eff}}}, \tag{5.5}$$

where

$$\boldsymbol{q}_{\text{eff}} \triangleq \boldsymbol{Q}^H_{\text{eff}} \boldsymbol{e}_{n_0}, \tag{5.6}$$

and

$$\boldsymbol{Q}_{\text{eff}} \triangleq \sum_{m=1}^{M} \boldsymbol{Q}_m. \tag{5.7}$$

The corresponding minimum error variance is obtained by the same replacements, respectively, in Eq. (3.23) as

$$\sigma^2_{e,\min} = 1 - \boldsymbol{q}^H_{\text{eff}} \left(\boldsymbol{Q}^H_{\text{eff}} \boldsymbol{Q}_{\text{eff}} + \sigma_c^2 \boldsymbol{\Phi}_{\text{eff}} \right)^{-1} \boldsymbol{q}_{\text{eff}}. \tag{5.8}$$

5.2 IIR Filter Optimization

Similarly, in the IIR case by replacing $Q_m(e^{j\omega})$, $\Phi_m(e^{j\omega})$, and $X(e^{j\omega})$ with

$$Q_{\text{eff}}(e^{j\omega}) \triangleq \sum_{m=1}^{M} Q_m(e^{j\omega}), \tag{5.9}$$

$$\Phi_{\text{eff}}(e^{j\omega}) = \sum_{m=1}^{M} \Phi_m(e^{j\omega}), \tag{5.10}$$

and

$$X_{\text{eff}}(e^{j\omega}) = \frac{|Q_{\text{eff}}(e^{j\omega})|^2}{\Phi_{\text{eff}}(e^{j\omega})}, \tag{5.11}$$

respectively, in Eqs. (3.44) and (3.45) we obtain

$$F_{\text{opt}}(e^{j\omega}) = \frac{1}{\alpha_{\text{opt}}^*} \frac{Q_{\text{eff}}(e^{j\omega})}{\Phi_{\text{eff}}(e^{j\omega})(\sigma_c^2 + X_{\text{eff}}(e^{j\omega}))} \tag{5.12}$$

$$\alpha_{\text{opt}} = \sqrt{\frac{1}{2\pi} \int_{-\pi}^{\pi} \frac{X_{\text{eff}}(e^{j\omega})}{(\sigma_c^2 + X_{\text{eff}}(e^{j\omega}))^2} \, \mathrm{d}\omega}. \tag{5.13}$$

The corresponding error variance is thus given by

$$\sigma_{e,\min}^2 = \frac{1}{2\pi} \int_{-\pi}^{\pi} \frac{\sigma_c^2}{\sigma_c^2 + X_{\text{eff}}(e^{j\omega})} \, \mathrm{d}\omega. \tag{5.14}$$

The approximate BER of the S–PEF scheme can be obtained by applying $\sigma_{e,\min}^2$ from Eq. (5.14) (or the corresponding expression for the FIR case) in Eq. (3.53)as

$$P_e = Q\left(\sqrt{2\left(\frac{1}{\sigma_{e,\min}^2} - 1\right)}\right). \tag{5.15}$$

Furthermore, we note that an uplink–downlink duality can also be established for the simplified MISO downlink structure and a corresponding simplified SIMO uplink configuration with just one post–equalization filter. Using similar steps as in Section 4.2 for the original transmitter structure, this duality can be exploited for adaptive calculation of the optimum PEF.

Chapter 6

Comparisons

It is of interest to compare the performances of the transmitter structure of the PEF scheme as in Fig. 2.1 and that of the S–PEF scheme in Fig. 5.1 for the IIR case. In the following section we compare the performances of these proposed schemes and discuss the trade–off between their computational complexity and system performance. On the other hand, we briefly discuss the previously proposed MMSE–Rake scheme in Section 6.2, and compare computational complexity of this scheme with that of the proposed PEF scheme.

6.1 PEF Scheme versus S–PEF Scheme

In order to compare the transmitter structures in Figs. 2.1 and 5.1, we first note that based on the complex version of Hölder's inequality [40] we can establish the following inequality

$$\left(\sum_{m=1}^{M} |\sqrt{\Phi_m(e^{j\omega})}|^2\right)^{1/2} \left(\sum_{m=1}^{M} \left|\frac{Q_m(e^{j\omega})}{\sqrt{\Phi_m(e^{j\omega})}}\right|^2\right)^{1/2} \geq \left|\sum_{m=1}^{M} Q_m(e^{j\omega})\right|. \qquad (6.1)$$

Squaring both sides of Eq. (6.1) and dividing them subsequently by $\sum_{m=1}^{M} \Phi_m(e^{j\omega})$ leads to

$$\frac{\left|\sum_{m=1}^{M} Q_m(e^{j\omega})\right|^2}{\sum_{m=1}^{M} \Phi_m(e^{j\omega})} \leq \sum_{m=1}^{M} \frac{|Q_m(e^{j\omega})|^2}{\Phi_m(e^{j\omega})}. \tag{6.2}$$

Therefore, we obtain

$$X_{\text{eff}}(e^{j\omega}) \leq X(e^{j\omega}), \tag{6.3}$$

where $X_{\text{eff}}(e^{j\omega})$ is defined in Eq. (5.11), and $X(e^{j\omega})$ is defined in Eq. (3.58). Since $X(e^{j\omega})$ and $X_{\text{eff}}(e^{j\omega})$ appear in the denominator of the respective error variances, Eq. (6.3) shows that the S–PEF scheme cannot outperform the PEF scheme. This result is not surprising since the S–PEF structure in Fig. 5.1 may be viewed as a special case of the PEF structure in Fig. 2.1 with $f_1[n] = f_2[n] = \cdots = f_M[n]$, $0 \leq n < L_f$. For the special case of an A–pre–Rake filter Eq. (6.3) simplifies to

$$\begin{aligned} X_{\text{eff}}(e^{j\omega}) &= \frac{1}{N} \sum_{m=1}^{M} \sum_{k=0}^{N-1} |\tilde{H}_m(e^{j(\omega-2\pi k)/N})|^2 \\ &= X(e^{j\omega}), \end{aligned} \tag{6.4}$$

It follows from Eq. (6.4) that the minimum error variances for the S–PEF scheme and the PEF scheme are equal in this case, cf. Eqs. (3.47), (5.14), i.e., both schemes will achieve the same performance. Therefore, the S–PEF scheme and the PEF scheme are equivalent for the IIR PEFs and A–pre–Rake combining, which implies that the S–PEF scheme should perform close to optimum as long as sufficiently long FIR PEFs and a good approximation of the A–pre–Rake filter (i.e., a P– or S–pre–Rake filter with a sufficient number of fingers) are employed. Thus, in this case, the more complex structure in Fig. 2.1 can be avoided. On the other hand, if a suboptimum pre–Rake filter with very few fingers and/or short FIR PEFs are used, the PEF structure in Fig. 2.1 is preferable and will lead to a better performance than the S–PEF structure in Fig. 5.1.

6.2 MMSE–Rake Scheme Versus PEF Scheme

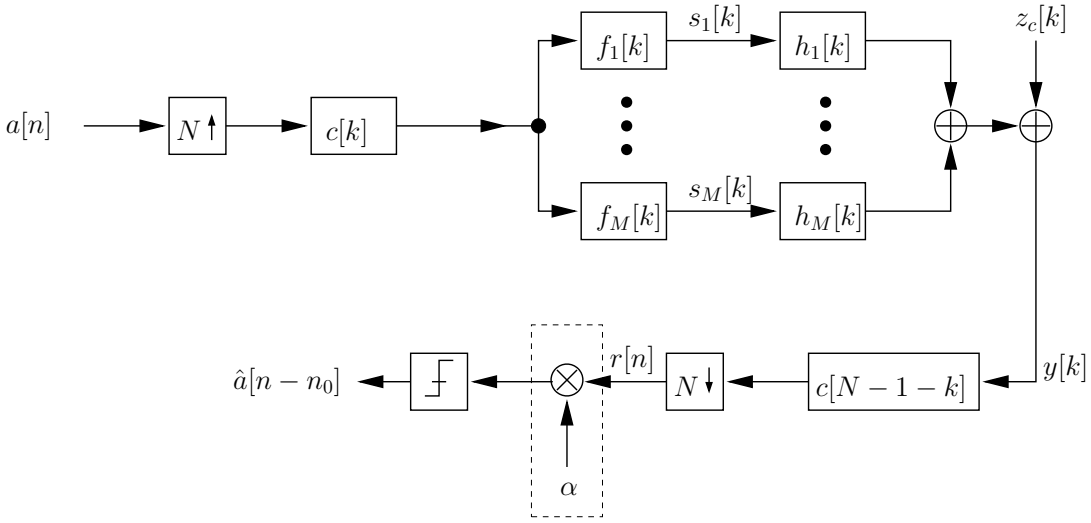

Figure 6.1: Block diagram of a MISO DS–UWB system with M transmit antennas, and a pre–equalization filter, implemented at chip level. The multiplication of $r[n]$ with α (dashed box) does not have to be implemented at the receiver, cf. discussion in Section 2.3 and Chapter 3.

In this section we briefly discuss the FIR pre–filtering method which was proposed in [24]. We call this method MMSE–Rake. We compare the performance of this scheme with that of our proposed PEF and S–PEF schemes in Chapter 7.

As in Chapter 2, we assume a MISO DS–UWB system with M transmit antennas. The transmitter structure of this system is shown in Fig. 6.1, in which the pre–Rake filter is replaced by a pre–equalization filter that minimizes the residual ISI at the receiver based on the MMSE criterion. Unlike our proposed method, this pre–filtering scheme is performed at the chip level. Note that all definitions are as in Chapter 3 unless they are redefined. Here, the resulting transmit symbol $s_m[k]$ is given by

$$s_m[k] = \sum_{i=-\infty}^{\infty} a[i]\tilde{f}_m[k - iN], \tag{6.5}$$

where $\tilde{f}_m[k] \triangleq c[k] * f_m[k]$. The received signal $r[n]$ can be expressed as

$$r[n] = \sum_{m=1}^{M} (\boldsymbol{Q}_{N,m} \boldsymbol{f}_m)^H \boldsymbol{a}[n] + z_s[n]$$

$$= (\boldsymbol{Q}_N \boldsymbol{f})^H \boldsymbol{a}[n] + z_s[n], \tag{6.6}$$

where $\boldsymbol{a}[n] \triangleq [a[n] \ \ldots \ a[n-L_t+1]]^T$, $\boldsymbol{f} \triangleq [\boldsymbol{f}_1^T \ \ldots \ \boldsymbol{f}_M^T]^T$, $\boldsymbol{f}_m \triangleq [f_m[0] \ \ldots \ f_m[L_f-1]]^H$, and $\boldsymbol{Q}_N \triangleq [\boldsymbol{Q}_{N,1} \ \ldots \ \boldsymbol{Q}_{N,M}]$, where $\boldsymbol{Q}_{N,m}$ denotes an $L_t \times L_f$ matrix defined as

$$\boldsymbol{Q}_{N,m} = \begin{bmatrix} q_m[k_0] & 0 & \ldots \\ q_m[N+k_0] & q_m[N+k_0-1] & \ldots \\ q_m[2N+k_0] & q_m[2N+k_0-1] & \ldots \\ \vdots & \vdots & \ldots \\ q_m[N(L_q-1)+k_0] & q_m[N(L_q-1)+k_0-1] & \ldots \\ 0 & \vdots & \ldots \\ \vdots & \vdots & \ldots \\ 0 & 0 & \ldots \end{bmatrix}. \tag{6.7}$$

Here, $q_m[k]$ is the overall CIR and is defined as

$$q_m[k] \triangleq c[k] * \tilde{h}_m[k], \tag{6.8}$$

where,

$$\tilde{h}_m[k] \triangleq h_m[k] * c[N-1-k], \tag{6.9}$$

and $L_t = \lceil (L_f + L_h + 2N - 3)/N \rceil$ is the length of the impulse response of the overall system which is the same as the length of the sampled overall CIRs, $q_m[Nn + k_0]$. The error variance at the receiver is the same as in Eq. (3.1). Applying Eq. (6.6) in Eq. (3.1) yields

$$\sigma_e^2 = 1 + |\alpha|^2 \sigma_c^2 - \alpha \boldsymbol{f}^H \boldsymbol{q} - \alpha^* \boldsymbol{q}^H \boldsymbol{f} + |\alpha|^2 \boldsymbol{f}^H \boldsymbol{Q}_N^H \boldsymbol{Q}_N \boldsymbol{f}, \tag{6.10}$$

where $\boldsymbol{q} \triangleq \boldsymbol{Q}_N^H \boldsymbol{e}_{n_0}$, and $\boldsymbol{e}_{n_0}$ denotes the unit vector whose elements are all zero except for the n_0th element which is equal to one. Furthermore, the error

variance σ_e^2 has to be minimized based on the MMSE criterion and subject to the average transmit power limit as

$$P \triangleq \sum_{k=Nn}^{N(n+1)-1} \sum_{m=1}^{M} \mathcal{E}\{|s_m[k]|^2\} = 1, \qquad \forall n. \tag{6.11}$$

Following the same steps as in Section 3.1 now we find a simpler constraint

$$P = \boldsymbol{f}^H \boldsymbol{f} = 1. \tag{6.12}$$

Combining Eqs. (6.10) and (6.12) we obtain the Lagrange problem as

$$L(\boldsymbol{f}, \alpha) = 1 + |\alpha|^2 \sigma_c^2 - \alpha \boldsymbol{f}^H \boldsymbol{q} - \alpha^* \boldsymbol{q}^H \boldsymbol{f} + |\alpha|^2 \boldsymbol{f}^H \boldsymbol{Q}_N^H \boldsymbol{Q}_N \boldsymbol{f} + \lambda(\boldsymbol{f}^H \boldsymbol{f} - 1), \tag{6.13}$$

where λ denotes the Lagrange multiplier. Similar to the steps made in Section 3.1, with differentiating $L(\boldsymbol{f}, \alpha)$ with respect to $\boldsymbol{f}^*$ and α^* and setting the resulting gradients to zero the optimum solution is obtained as

$$\boldsymbol{f}_{\text{opt}} = \frac{1}{\alpha_{\text{opt}}^*} \left(\boldsymbol{Q}_N^H \boldsymbol{Q}_N + \sigma_c^2 \boldsymbol{I} \right)^{-1} \boldsymbol{q} \tag{6.14}$$

$$\alpha_{\text{opt}} = \sqrt{\boldsymbol{q}^H \left(\boldsymbol{Q}_N^H \boldsymbol{Q}_N + \sigma_c^2 \boldsymbol{I} \right)^{-2} \boldsymbol{q}}. \tag{6.15}$$

Since MMSE pre–filtering is implemented at the chip level, long filters may be necessary depending on the underlying channel in order to achieve a good performance. Eq. (6.14) shows that for long filter lengths the computation of the filter coefficients requires the inversion of a matrix with a size equal to the filter length and therefore, entails a high complexity. However, in our proposed methods the pre–equalization filters are implemented at the symbol level, which brings much less computational complexity. Numerically, in the MMSE–Rake scheme $\boldsymbol{Q}_N$ is of size $L_t \times ML_f$, where $L_t = \lceil (L_f + L_h + 2N - 3)/N \rceil$, and $\boldsymbol{Q}_N^H \boldsymbol{Q}_N$ in Eq. (6.14) is of size $ML_f \times ML_f$, where $L_f \approx L_h$ (or even $> L_h$), while in our proposed PEF scheme $\boldsymbol{Q}$ is of size $L_t \times ML_f$, where $L_t = \lceil (L_g + L_h + 2N - 3)/N \rceil + L_f - 1$, and therefore $\boldsymbol{Q}^H \boldsymbol{Q}$ in Eq. (3.20) is of size $ML_f \times ML_f$, and L_f is quite small. Since the computational complexity of inverting an $n \times n$ matrix is of the order of $O(n^3)$, one can observe that

Eq. (3.20) is far less complex than Eq. (6.14). In Chapter 7, the performance of the MMSE–Rake is compared with that of our proposed PEF schemes for the UWB channel models CM1 and CM4.

Chapter 7

Simulation and Numerical Results

In this chapter, we present computer simulation and numerical results for the proposed PEF schemes for MISO DS–UWB systems. In particular, we show results for the effective SNR at the receiver and the BER. Thereby, we consider the practically most relevant cases of $M = 1$ and $M = 2$ transmit antennas. For convenience and practical relevance, we adopted for our simulations the parameters from the IEEE 802.15.3a standardization efforts. In particular, we assume a chip duration of $T_c = 0.76$ ns and both transmit filter $g_T(t)$ and receive filter $g_R(t)$ are square-root raised-cosine filters with rolloff factor 0.3 [41]. For $M = 2$ transmit antennas we assumed that the log–normal terms X_m, $m \in \{1, 2\}$, are correlated with correlation coefficient $\rho_X = 0.86$ [31]. We focus on the CM1 and CM4 channel models as they have the smallest and the largest average delay spread of the four channel models proposed in [29, 30], respectively. All effective SNR and BER results shown in the following were averaged over 100 channel realizations. For our simulations, we generated oversampled versions of $\acute{h}_m(t)$, $h_m(t)$, $g_T(t)$, and $g_R(t)$ with a sampling interval of $T_c/8$, respectively. The oversampled overall CIR was then downsampled and the resulting overall discrete-time CIR was truncated to length L_h such that

$\sum_{k=0}^{L_h-1} \mathcal{E}\left\{|h_m[k]|^2\right\} / \sum_{k=-\infty}^{\infty} \mathcal{E}\left\{|h_m[k]|^2\right\} < 0.999$. This led to $L_h = 145$ and $L_h = 420$ for CM1 and CM4, respectively. Throughout this chapter we adopt for the sampling phase $k_0 = k_0^s$, cf. Section 2.3, and for FIR PEFs the decision delay n_0 was optimized. Finally, we will show the BER sensitivity of our proposed system to imperfect CSI estimation.

7.1 Effective SNR Results

First, we show numerical results for the average effective SNR at the receiver by averaging $\text{SNR} = 1/\sigma^2_{e,\min} - 1$ over 100 independent channel realizations (cf. Fig. 2.2, 2.3). Thereby, $\sigma^2_{e,\min}$ is obtained from the analytical expressions in Eqs. (3.23), (3.47), and (5.14).

Fig. 7.1 shows the average effective SNR of the PEF and S–PEF schemes with A–pre–Rake combining vs. FIR PEF length L_f for the CM1 channel model, for $M = 2$, $N = 6$, and $E_b/N_0 = 15$ dB, where E_b and N_0 denote the average energy per bit and the single–sided power spectral density of the underlying passband AWGN process, respectively. Fig. 7.1 shows that as L_f increases the FIR PEF filters quickly approach the performance of IIR PEF filters (solid lines). The performance of IIR PEF filters can be achieved by employing $L_f = 40$ for this channel model. We also note that while the PEF scheme achieves a higher SNR than the S–PEF scheme for short FIR PEFs, both schemes achieve the same performance for long FIR and IIR filters, cf. Section 6.1.

For comparison, we have also included in Fig. 7.1 the results for the MMSE–Rake scheme proposed in [24]. As L_f increases the MMSE–Rake scheme achieves the same performance as the proposed PEF and S–PEF schemes. However, since the filters in the MMSE–Rake scheme operate at the chip level, the convergence to the optimum IIR performance is much slower than for the PEF and S–PEF schemes. For example, if an SNR of 14 dB is desired for CM1,

the PEF and the MMSE–Rake schemes require filter lengths of 4 and 114, respectively. Asymptotically, using the MMSE–Rake scheme, the performance of IIR can be achieved by having $L_f = 200$ for CM1 compared to $L_f = 40$ for the PEF scheme. Later on, we will show that even much smaller numbers of L_f for the PEF scheme can achieve a very good BER performance compared to MMSE–Rake scheme.

Fig. 7.2 shows the average effective SNR of the PEF and the S–PEF scheme

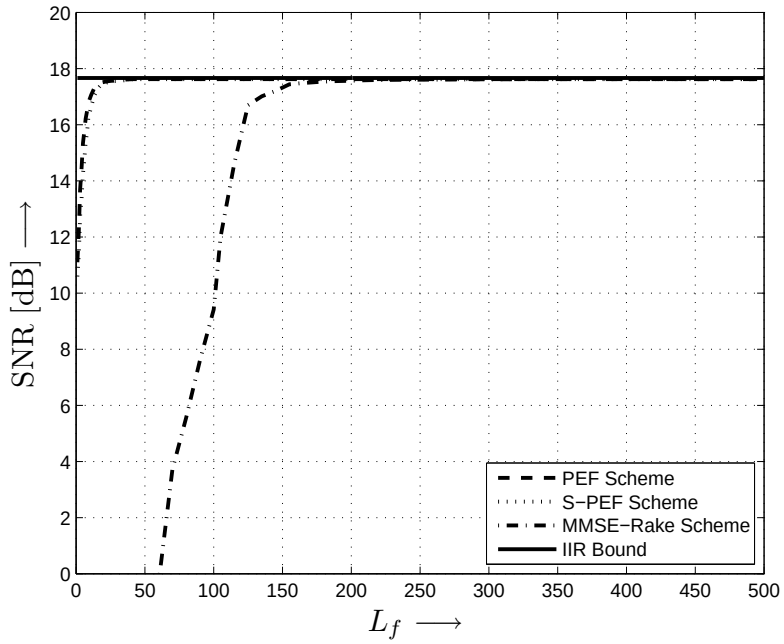

Figure 7.1: Effective SNR vs. L_f for PEF, S–PEF, and MMSE–Rake schemes for CM1 UWB channel model. A–pre–Rake, $M = 2$, $N = 6$, and $E_b/N_0 = 15$ dB.

with A–pre–Rake combining vs. FIR PEF length L_f for CM4. Similar to the CM1 channel model, as L_f increases the FIR PEF filters quickly approach the performance of IIR PEF filters (solid lines). Since the average delay spread for CM4 is considerably larger than for CM1, this convergence is much slower for CM4 than for CM1. The performance of IIR PEF filters can be achieved by employing a filter length of at least $L_f = 90$ for CM4.

Again, we have included in Fig. 7.2 the results for the MMSE–Rake scheme.

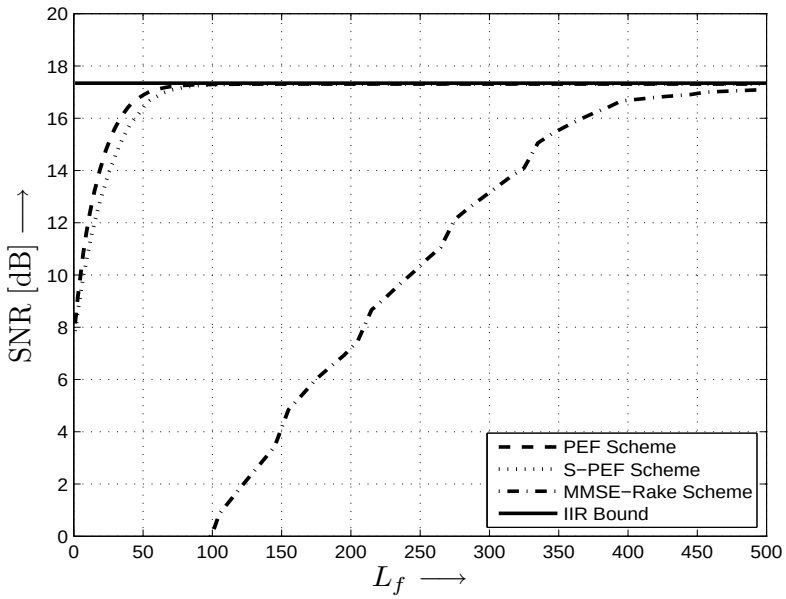

Figure 7.2: Effective SNR vs. L_f for PEF, S–PEF, and MMSE–Rake schemes for CM4 UWB channel model. A–pre–Rake, $M = 2$, $N = 6$, and $E_b/N_0 = 15$ dB.

The convergence to the optimum IIR performance is much slower than for the PEF and the S–PEF scheme. As can be seen from the figure, for CM4 we need a filter length of more than 500 to achieve the performance of the IIR case, compared to $L_f = 90$ for the PEF scheme. The computation of the long filters required for the MMSE–Rake may be very difficult in practice even if a recursive (e.g. a steepest descent algorithm) or an adaptive algorithm (e.g. LMS algorithm) is used to avoid direct matrix inversion.

In Figures 7.3 and 7.4, we investigate the dependence of the average effective SNR of the PEF and the S–PEF scheme on the spreading factor N for CM1 and CM4, respectively, for $M = 2$, $L_f = 5$, $E_b/N_0 = 15$ dB, and A–pre–Rake combining are assumed. For both CM1 and CM4, as N increases the effective amount of ISI after pre–Rake combining rapidly decreases, and both the PEF and the S–PEF scheme approach the SNR of the pure AWGN channel given by SNR $= M/\sigma_c^2$ (solid line), cf. Section 3.6.

Again the convergence to the optimum value is slower for CM4 than for CM1

because of its larger delay spread. The performance of the pure AWGN

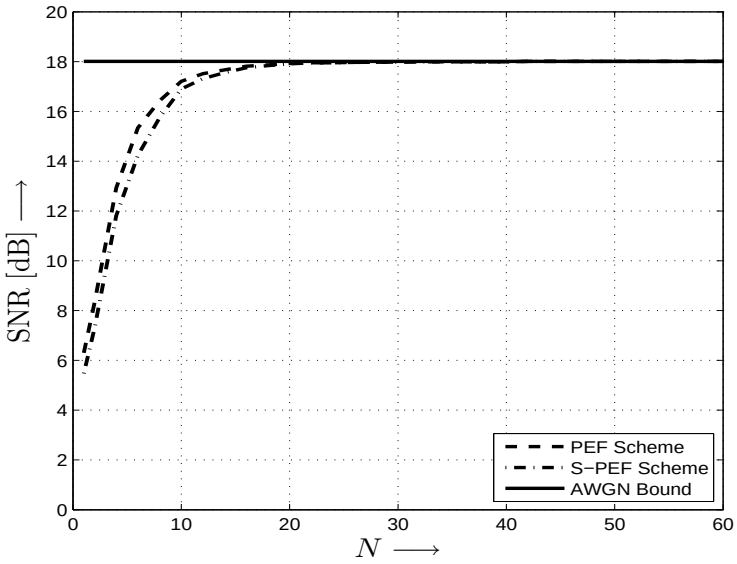

Figure 7.3: Effective SNR vs. N for PEF and S–PEF schemes for CM1 model. A–pre–Rake, $M = 2$, $L_f = 5$, and $E_b/N_0 = 15$ dB.

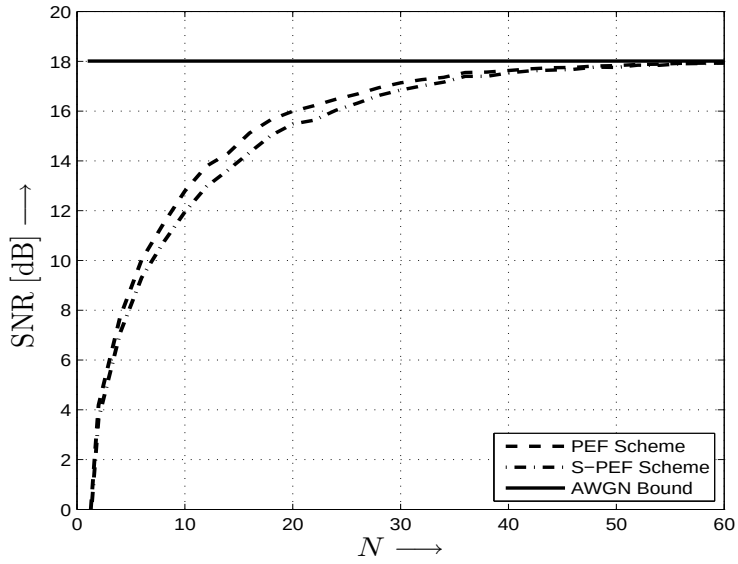

Figure 7.4: Effective SNR vs. N for PEF and S–PEF schemes for CM4 model. A–pre–Rake, $M = 2$, $L_f = 5$, and $E_b/N_0 = 15$ dB.

channel can practically be achieved by using $N = 20$ for CM1, while we need

at least $N = 50$ to achieve the same performance for CM4. Note again that the PEF scheme outperforms the S–PEF scheme for small values of N.

The average effective SNR of the PEF and the S–PEF scheme as a function of L_f for CM1 and CM4 are shown in Figs. 7.5 and 7.6, respectively, this time for A–pre–Rake combining and S–pre–Rake combining with different numbers of fingers S ($M = 2$, $N = 6$, and $E_b/N_0 = 15$ dB). As predicted in Section 5.2,

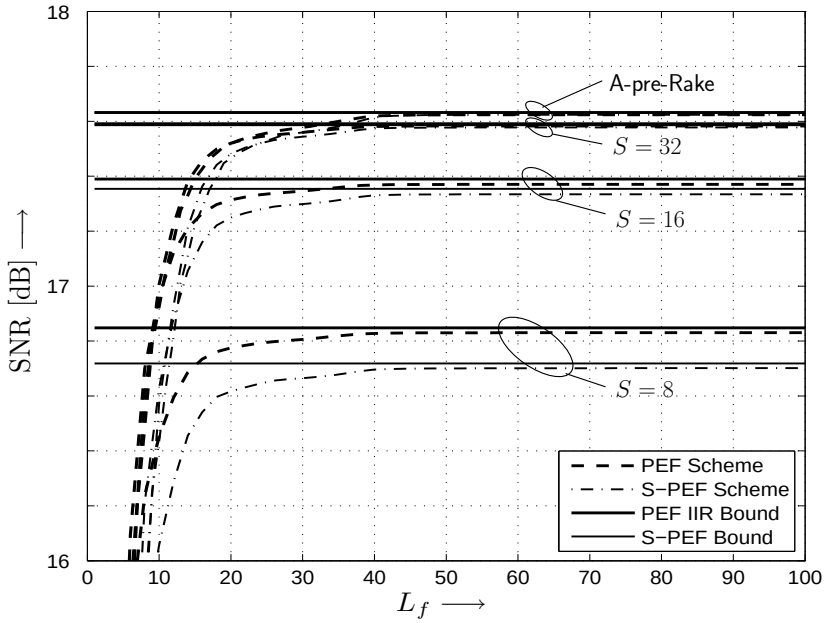

Figure 7.5: Effective SNR vs. L_f for PEF and S–PEF schemes for CM1 UWB channel model. S–pre–Rake, $M = 2$, $N = 6$, and $E_b/N_0 = 15$ dB.

with S–pre–Rake combining the PEF scheme outperforms the S–PEF scheme even for IIR PEFs and the performance gap between both schemes increases as the number of fingers decreases. Numerical results show that, for CM1, the asymptotic SNR differences between the PEF and the S–PEF scheme for $S = 32$, 16, and 8 are 0.005 dB, 0.04 dB, and 0.13 dB, respectively.

As can be seen in Fig. 7.6 for CM4, the asymptotic SNR differences between the PEF and the S–PEF scheme are slightly higher, namely 0.25 dB, 0.60 dB, and 1.14 dB, for $S = 32$, 16, and 8, respectively.

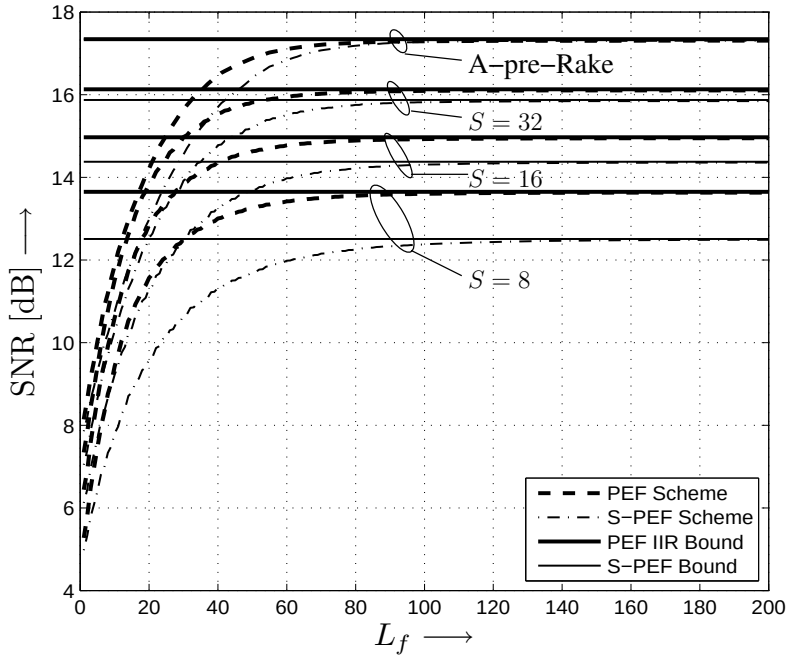

Figure 7.6: Effective SNR vs. L_f for PEF and S–PEF schemes for CM4 UWB channel model. S–pre–Rake, $M = 2$, $N = 6$, and $E_b/N_0 = 15$ dB.

7.2 BER Results

Now, we show simulation and numerical results for the BER of the PEF and the S–PEF scheme. Fig. 7.7 shows simulated BER results for the PEF and the S–PEF scheme with FIR PEFs of lengths $L_f = 5$, 10, and 20 for CM1, and numerical results for the same schemes with IIR PEFs obtained from Eq. (3.53). $M = 2$, $N = 6$, and A–pre–Rake combining are used. For comparison we also show simulation results for the A–pre–Rake (or time–reversal) scheme without pre–equalization and the MF bound calculated based on Eq. (3.61). As can be observed from Fig. 7.7, both the PEF and the S–PEF scheme significantly lower the high BER floor of the pure A–pre–Rake scheme. The performance gap between the PEF scheme and the S–PEF scheme decreases as L_f increases and disappears for $L_f \to \infty$ as expected from the discussion in Section 5.2. We note that the gap between IIR PEFs and the MF bound is only 0.3–dB in this case.

Fig. 7.8 shows simulated BER results for the PEF and the S–PEF scheme

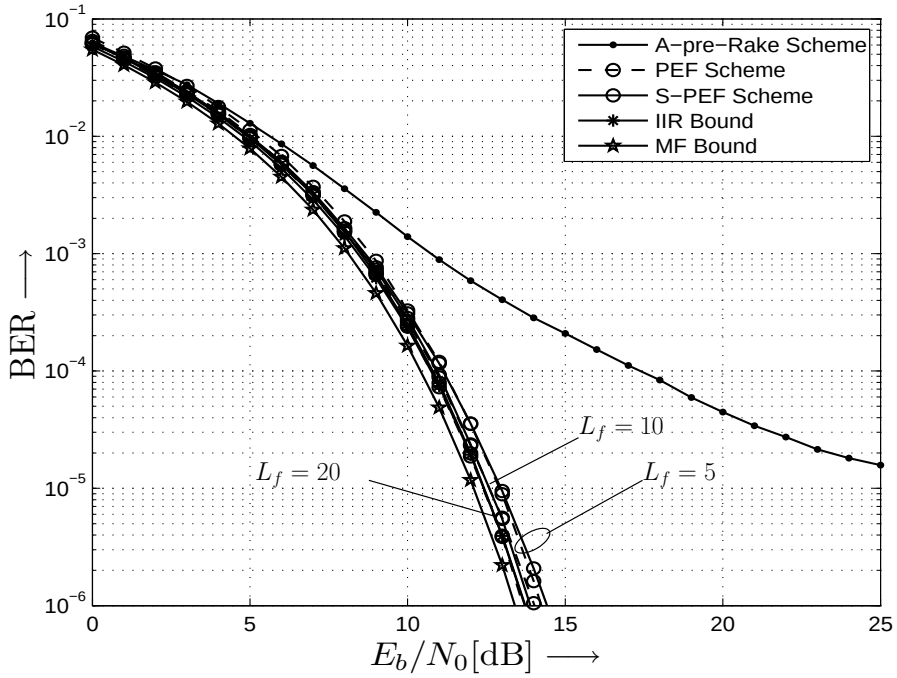

Figure 7.7: BER vs. E_b/N_0 for PEF, S–PEF, and A–pre–Rake schemes for CM1. A–pre–Rake, $M = 2$, and $N = 6$. MF bound is also shown.

with FIR PEFs of lengths $L_f = 5$, 10, and 20 for CM4. Again, both the PEF and the S–PEF scheme significantly lower the high BER floor of the pure A–pre–Rake scheme as in CM1. The performance gap between the PEF scheme and the S–PEF scheme decreases as L_f increases and disappears for $L_f \to \infty$ (cf. Section 6.1). We note that even for IIR PEFs there remains a 1–dB gap to the MF bound. However, to further narrow this gap some form of non–linear processing at the transmitter would be required, which would (further) increase complexity.

In Fig. 7.9, we compare the performances of the PEF scheme for $M = 1$ and $M = 2$ transmit antennas. We assume S–pre–Rake combining with $S = 16$ fingers and $N = 6$ and we investigate CM1. The BER curves for the FIR PEFs and the S–pre–Rake scheme without equalization were simulated, whereas the BER curves for the IIR PEFs and the MF bound were obtained by evaluating

Eqs. (3.53) and (3.61), respectively. Fig. 7.9 shows that a second transmit antenna yields substantial performance improvements even if the antennas are correlated due to the correlated log–normal shadowing terms. This performance gain is about 4.1 dB at the bit error rate of 10^{-3} for IIR PEFs, and even larger gains are obtained for short FIR PEFs. These gains are due to the fact that increasing M has a similar effect as increasing the spreading factor N, cf. Section 3.6.

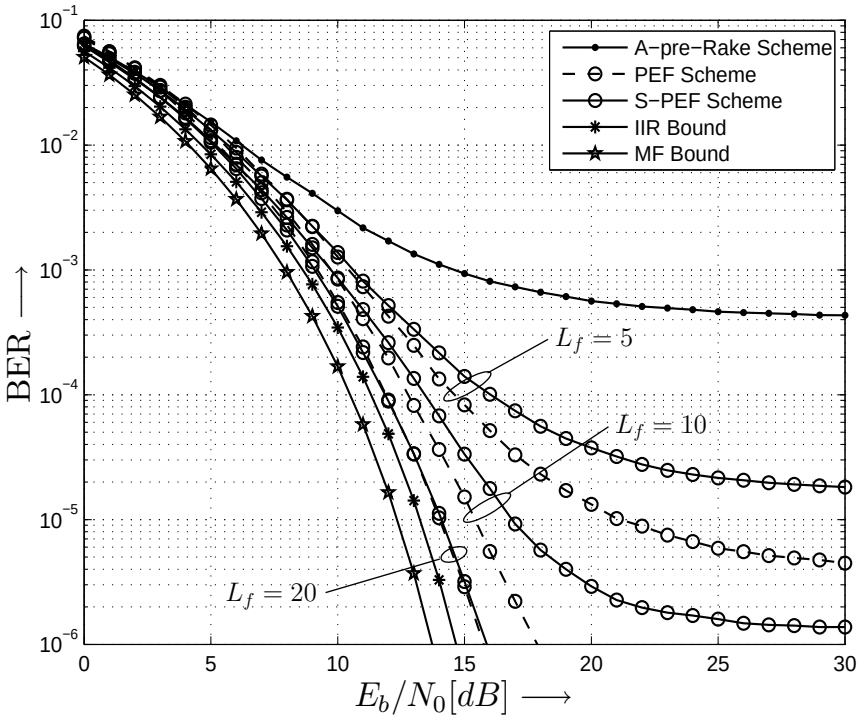

Figure 7.8: BER vs. E_b/N_0 for PEF, S–PEF, and A–pre–Rake schemes for CM4. A–pre–Rake, $M = 2$, and $N = 6$. MF bound is also shown.

Fig. 7.10, shows the same comparison between the performances of the PEF scheme for $M = 1$ and $M = 2$ transmit antennas for CM4. The positive effects of increasing the length of the filters L_f and the number of antennas M on the performance can still be observed in this case. However, the performance improvement from $L_f = 5$ to $L_f = 10$, and $L_f = 20$ is much more evident compared to CM1. This is because of the relatively larger delay spread of

CM4, which requires longer PEFs. Again, the second transmit antenna yields a substantial performance gain of about 3.8 dB at the bit error rate of 10^{-3} for IIR PEFs, and even larger gains are obtained for short FIR PEFs. Remarkably, even if we fix the total number of FIR filter taps ML_f, the SISO scheme with $L_f = 10$ and $L_f = 20$ still performs substantially worse than the MISO scheme with $L_f = 5$ and $L_f = 10$, respectively. Note that larger PEFs are required to achieve a performance close to the IIR, but increasing number of antennas from $M = 1$ to $M = 2$ decreases the performance gap between FIR PEF and IIR PEF significantly. The relatively large gap between the MF bounds and the corresponding PEF scheme with IIR filters is due to the suboptimum S–pre–Rake combining.

In Fig. 7.11, we compare the performance of the PEF and the S–PEF scheme

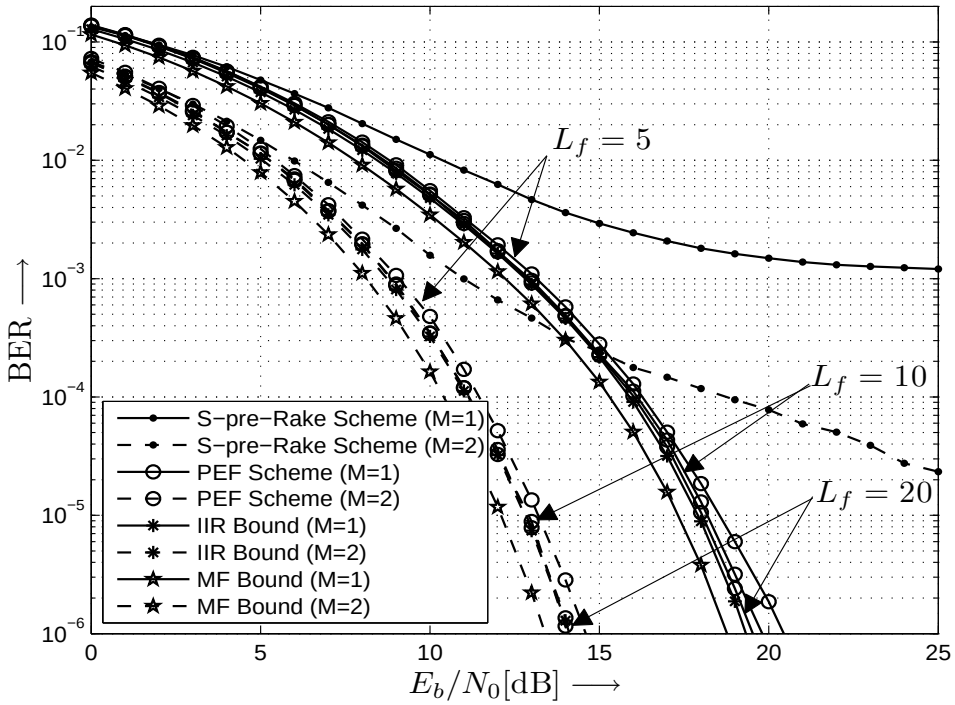

Figure 7.9: BER vs. E_b/N_0 for PEF and S–pre–Rake schemes for CM1. S–pre–Rake with $S = 16$ fingers and $N = 6$. MF bounds are also shown.

for CM1, for different spreading factors N assuming S–pre–Rake combining

($S = 16$) and $M = 2$. For FIR PEFs with $L_f = 10$ both simulation (markers) and analytical (lines) results obtained from Eq. (3.53) are shown. For IIR PEFs only analytical results for $N = 12$ are shown. For both the FIR PEF and the FIR S–PEF scheme the analytical and simulation results are in good agreement for sufficiently large spreading factors N, i.e., for $N = 6, 12$. Furthermore, since the amount of ISI after pre–Rake combining decreases as N increases, the performance of both the PEF and S–PEF schemes improves and the gap between both schemes decreases with increasing N. Of course, this performance improvement comes at the price of a decreased data rate. We note that since S–pre–Rake combining is used the PEF scheme outperforms the S–PEF scheme even for IIR PEFs, cf. Section 5.2. The same comparison

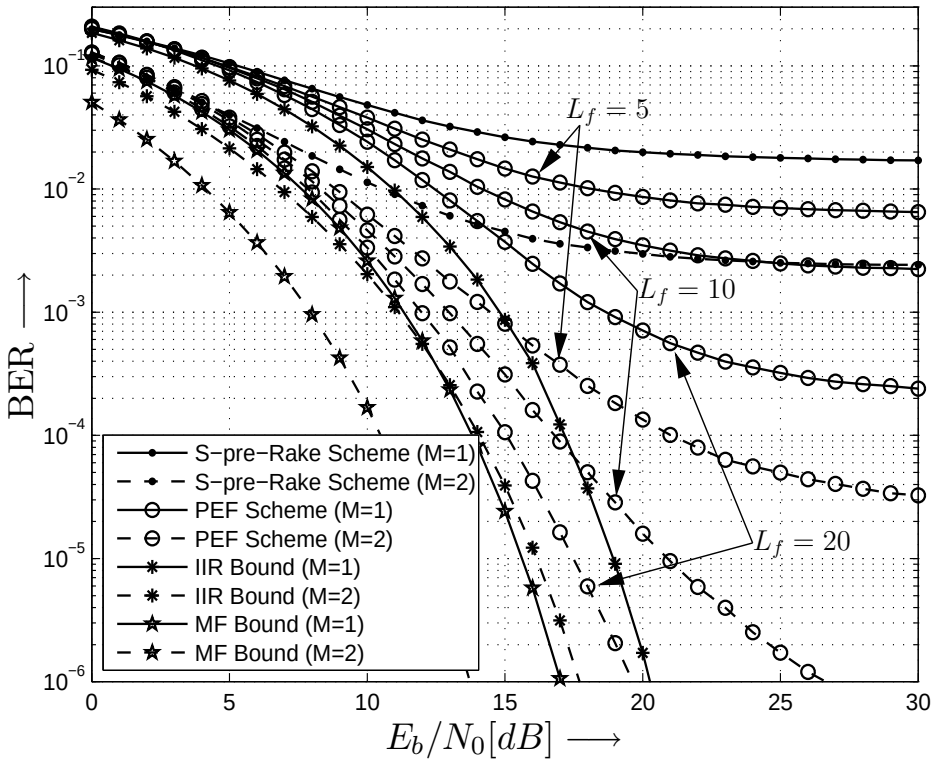

Figure 7.10: BER vs. E_b/N_0 for PEF and S–pre–Rake schemes for CM4. S–pre–Rake with $S = 16$ fingers and $N = 6$. MF bounds are also shown.

for the performance of the PEF and the S–PEF scheme for CM4 are shown in

Fig. 7.12, again for different spreading factors N assuming S–pre–Rake combining ($S = 16$) and $M = 2$. For IIR PEFs only analytical results for $N = 12$ are shown. We observe that for both the FIR PEF and the FIR S–PEF the analytical and simulation results are in good agreement in this case, even for smaller spreading factor $N = 3$. Note that the PEF scheme with small number of filter coefficients, i.e., $L_f = 10$ can suppress some ISI, while leaving some residual interference. To obtain the BER expression in Eq. (3.53) we used the central limit theorem and assumed that the residual interference term in Eq. (3.48) is approximately Gaussian distributed. Since CM4 has longer delay spread than CM1 this approximation is more valid for CM4.

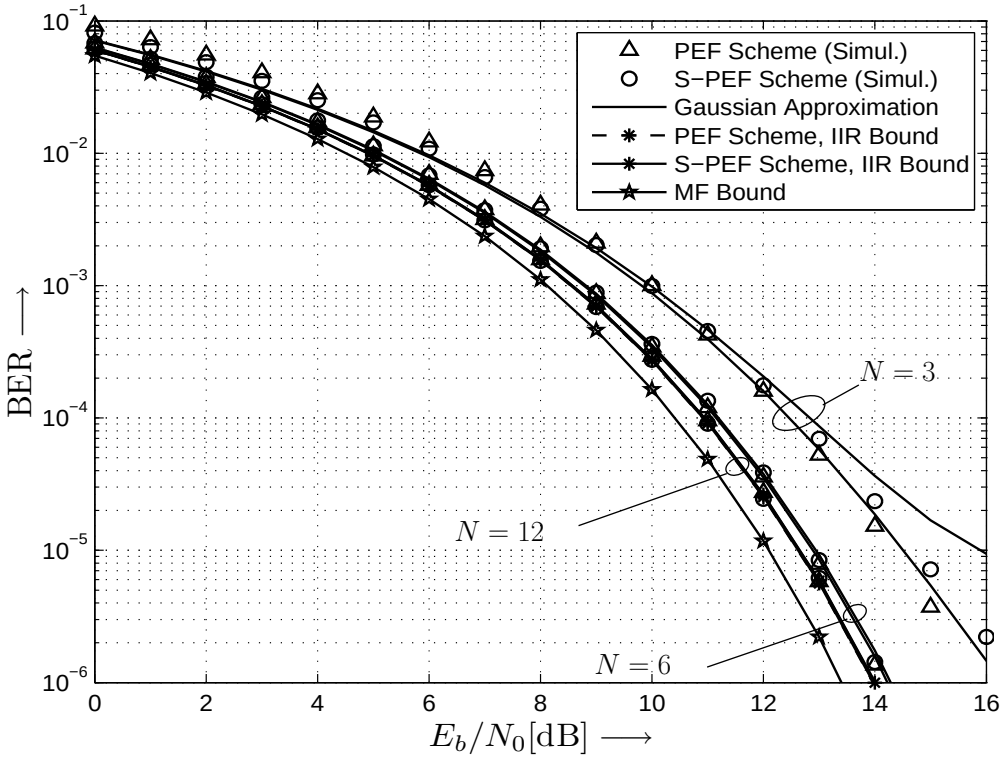

Figure 7.11: BER vs. E_b/N_0 for PEF and S–PEF schemes for CM1. S–pre–Rake with $S = 16$ fingers, $M = 2$, and $L_f = 10$. MF bound is also shown.

Finally, in Figs. 7.13 and 7.14, we compare the BER performance of the PEF scheme with that of the previously proposed MMSE–Rake scheme, for CM1

and CM4. A–pre–Rake combining and $M = 2$ are assumed. For this purpose we show the performance of the PEF scheme with $L_f = 10$, and $L_f = 30$ for CM1 and CM4, respectively. To clarify how we choose the length of the filter L_f for the PEF scheme and the MMSE–Rake scheme, we refer to Figs. 7.1 and 7.2. It can be observed in Fig. 7.1 that for CM1 the PEF scheme requires filter length of $L_f = 10$ to achieve SNR = 16.9 dB, while the MMSE–Rake scheme requires $L_f = 145$ to achieve SNR = 17.2 dB, therefore for CM1, the PEF scheme with $L_f = 10$ and the MMSE–Rake scheme with $L_f = 145$ are compared in Fig. 7.13. Note that we choose these values since we want to show close–to–optimum performances for both cases and we also intend to show the performance that the MMSE–Rake can achieve with long filter length equal to the length of the channel, i.e., $L_f = 145$.

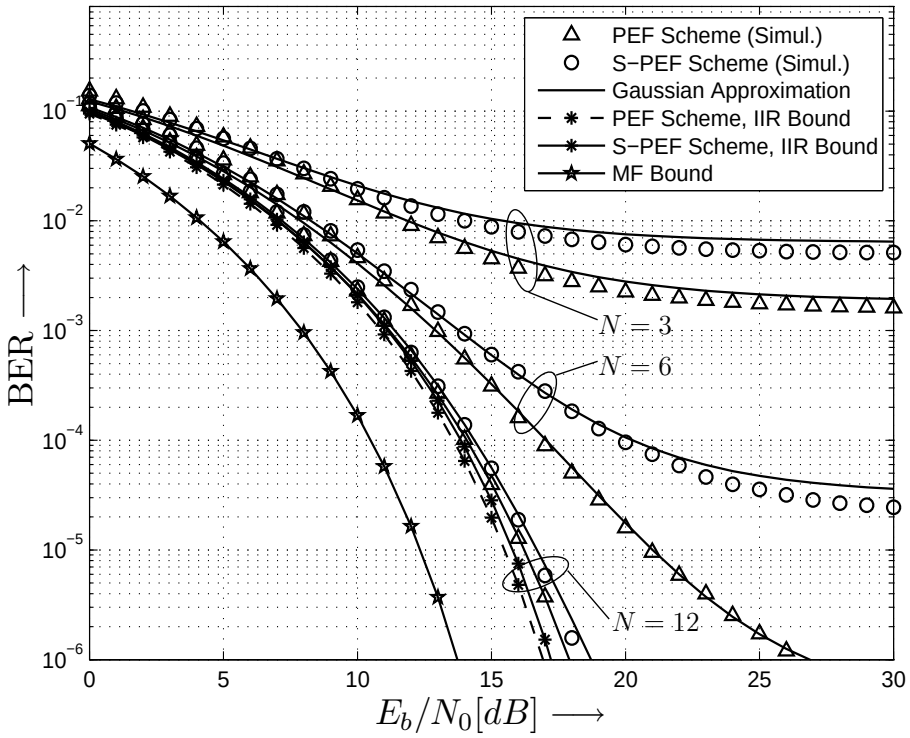

Figure 7.12: BER vs. E_b/N_0 for PEF and S–PEF schemes for CM4. S–pre–Rake with $S = 16$ fingers, $M = 2$, and $L_f = 10$. MF bound is also shown.

Following a similar discussion for CM4, Fig. 7.2 shows that the PEF scheme

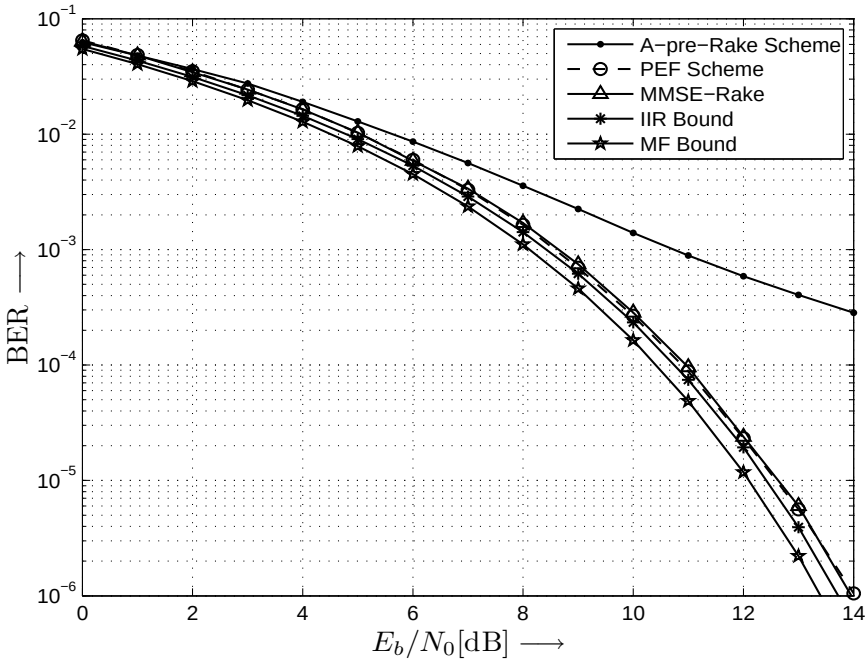

Figure 7.13: BER vs. E_b/N_0 for PEF with $L_f = 10$ and MMSE–Rake schemes for CM1. A–pre–Rake and $M = 2$ are assumed. MF bound is also shown.

with $L_f = 30$ is required to achieve SNR = 15.6, while the MMSE–Rake scheme requires $L_f = 420$ to achieve SNR = 16.8 dB. Therefore, the PEF scheme with $L_f = 30$ and the MMSE–Rake scheme with $L_f = 420$ are compared in Fig. 7.14. Note that we could choose a shorter filter length for the MMSE–Rake scheme to achieve closer BER performance to that of the PEF scheme but again, we intend to show the performance that the MMSE–Rake can achieve with long filter length equal to the length of the channel, i.e. $L_f = 420$. As we expected from the simulation results in Section 7.1, Figs. 7.13 and 7.14 show that even with very small filter length of $L_f = 10$, and $L_f = 30$ for CM1 and CM4, respectively, the PEF scheme can closely achieve the same performance of MMSE–Rake scheme. Note that the small performance gap between the PEF scheme and the MMSE–Rake scheme in Fig. 7.14 can be reduced by slightly increasing L_f in the PEF scheme. However as shown in Section 6.2 the computational complexity of the PEF scheme is significantly lower than that of the MMSE–Rake scheme. For the PEF scheme the computation of the

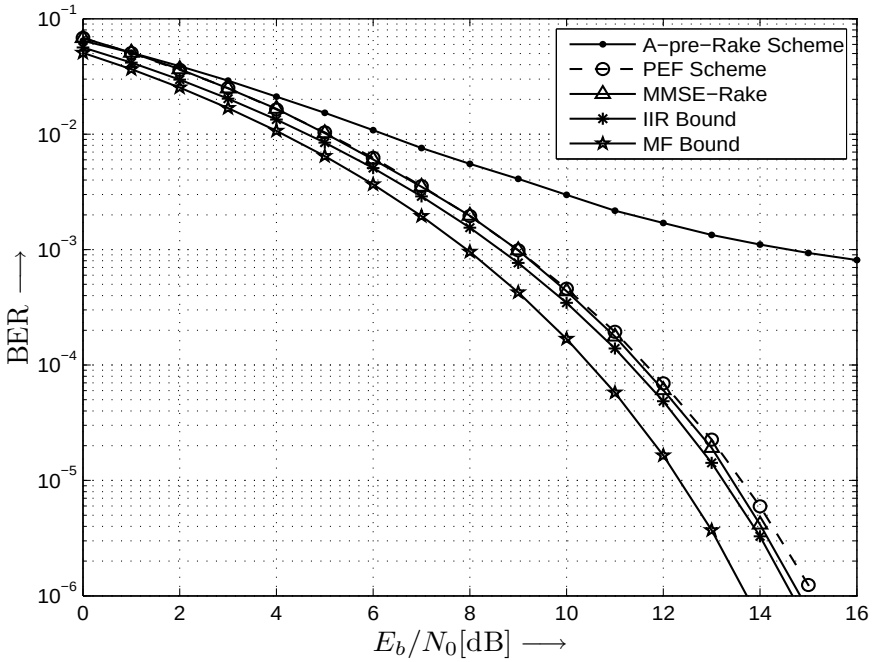

Figure 7.14: BER vs. E_b/N_0 for PEF with $L_f = 30$ and MMSE–Rake schemes for CM4. A–pre–Rake and $M = 2$ are assumed. MF bound is also shown.

filter coefficients requires the inversion of a matrix with a size equal to the filter length which are 10 and 30 for CM1 and CM4, respectively, while in the case of the MMSE–Rake scheme the size of this matrix is 145 and 420 for CM1 and CM4, respectively.

7.3 CSI Sensitivity Results

Throughout this work Rake combining has been used to reduce the multipath fading in the UWB system. However, the tap weights of the multipath channel model, also known as CSI, need to be estimated. We assumed that perfect CSI is available at the transmitter for the downlink structure, and at the receiver for the dual uplink structure. We also assumed the use of time–division duplex (TDD), in which the same frequency band is used for both the uplink and downlink by switching between transmission and reception in time,

and exploited the fact that the UWB radio channel is reciprocal [19].

In practice, the CSI should be estimated at the receiver or the transmitter. There are different methods for channel estimation such as the synchronized summation scheme [18]. We do not intend to cover these methods here, instead, we briefly show the sensitivity of our proposed methods to imperfect CSI. To demonstrate the effect of imperfect CSI, we assume that instead of having the perfect CIRs available, we only have a noise corrupted version of the CIRs at the transmitter, considering the downlink structure. For this purpose, consider again the system model depicted in Fig. 2.1. The estimated CIRs at the transmitter, $\hat{h}_m[k]$ is defined according to

$$\hat{h}_m[k] = h_m[k] + e_m[k], \tag{7.1}$$

where $h_m[k]$ is the true base–band discrete–time CIRs as defined in Section 2.2, and $e_m[k]$ are i.i.d. AWGN samples with variance σ_e^2 at antenna m, $1 \leq m \leq M$. We define the variance of the impacting noise as a fraction of the system noise according to

$$\sigma_e^2 = \beta \cdot \sigma_c^2, \tag{7.2}$$

where σ_c^2 denotes the variance of the chip–level AWGN at the receiver as defined in Section 2.2. β is defined as the sensitivity factor, and we consider the cases $\beta = 0$ (perfect CSI), and $\beta = 0.001$, 0.01, and 0.1.

Figs. 7.15 and 7.16, show the BER performance of CM1 and CM4, respectively, in the presence of imperfect CSI. S–pre–Rake with $S = 16$ fingers, $N = 6$, $M = 2$, and $L_f = 20$ are assumed, and both PEF and S–PEF schemes are examined in theses simulations.

Fig. 7.15 shows that for CM1, even for a relatively high sensitivity factor of $\beta = 0.1$, the system performance for the PEF and the S–PEF scheme is quite close to the case of perfect CSI with $\beta = 0$, and suffers a performance loss of only 0.25 dB at the bit error rate of 10^{-4}.

Fig. 7.16 shows the BER performance for the PEF and the S–PEF scheme

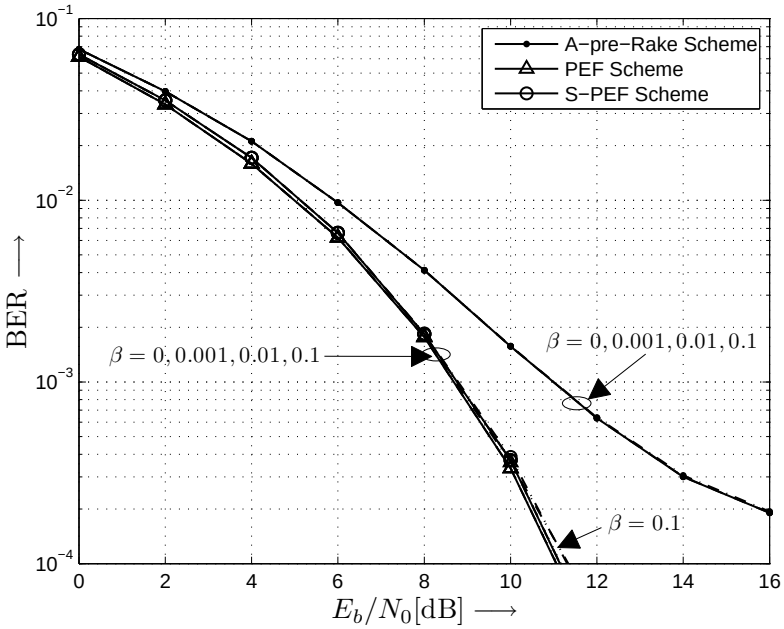

Figure 7.15: BER vs. E_b/N_0 for PEF and S–PEF schemes for CM1. S–pre–Rake with $S = 16$ fingers, $M = 2$, and $L_f = 20$. Sensitivity factor $\beta = 0, 0.001, 0.01, 0.1$.

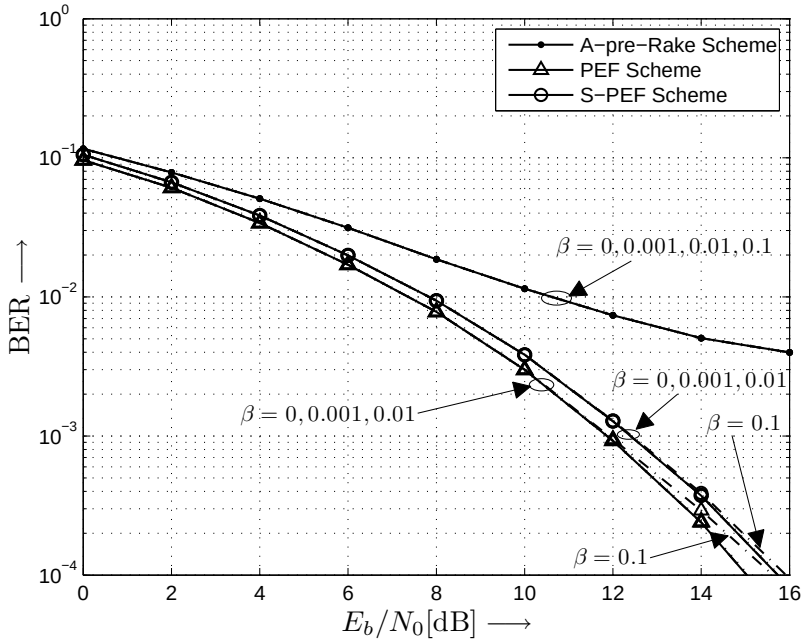

Figure 7.16: BER vs. E_b/N_0 for PEF and S–PEF schemes for CM4. S–pre–Rake with $S = 16$ fingers, $M = 2$, and $L_f = 20$. Sensitivity factor $\beta = 0, 0.001, 0.01, 0.1$.

for CM4. Still, for a relatively high sensitivity factor of $\beta = 0.1$, the system performance loss is less than 1 dB at the bit error rate of 10^{-4}. Particularly, we observe that at higher SNR the S–PEF scheme has less performance loss compared to the PEF scheme and is more robust to imperfect CSI.

Chapter 8

Conclusions and Future Work

This chapter concludes the thesis with some general comments on pre–equalization for pre–Rake MISO DS–UWB systems proposed in this work, followed by a discussion on possible future work for further investigation.

8.1 Conclusions

In this work, we have proposed two different PEF schemes for MISO DS–UWB systems with pre–Rake combining. The first PEF scheme employs one PEF per transmit antenna, whereas the second, simplified scheme requires only one PEF shared by all transmit antennas. In contrast to previously proposed pre–filtering schemes for DS–UWB, both proposed PEF schemes efficiently exploit the channel shortening properties of the pre–Rake filter and operate at the symbol level. Therefore, relatively short PEFs achieve close–to–optimum performance even for long UWB CIRs. For sufficiently long PEFs and A–pre–Rake combining both proposed PEF schemes achieve the same performance, but the S–PEF scheme suffers from a certain performance degradation for suboptimum pre–Rake combining and/or short PEFs. Furthermore, we have also shown that a SIMO DS–UWB system with post–Rake combining and

MMSE post–equalization is the dual system for our MISO DS–UWB system with pre–Rake combining and MMSE pre–equalization. This uplink–downlink duality can be exploited for complexity reduction. Simulation results have confirmed the analytical findings and the excellent performance of the proposed PEF schemes. We note that while in this paper only DS–UWB systems have been considered, the proposed PEF schemes are also applicable to other areas (e.g. TDD–CDMA systems and underwater acoustic communication) where pre–Rake combining is used.

8.2 Recommendations for Future Work

We believe that the research work we initiated here on pre–equalization for MISO DS–UWB systems with pre–Rake combining only scratches the tip of the iceberg and many important questions remain to be answered. We list some recommendations for future work as follows:

- In this work, we did not consider the effect of multiuser interference (MUI). An extension to the present work could be the study of the multiusers case, which we expect to impact our proposed PEF and S–PEF schemes. Since we have already included spreading sequences in our work, this extension could be easily done.

- We did not consider the FCC power spectrum limitation in our proposed filter optimization method. In addition to the transmit signal average power constraint, limiting the spectrum of the transmit signal will introduce additional constraints to the present optimization problem, and could be an interesting topic for future work.

- Last but not least, employing the non–linear processing at the transmitter (e.g. Tomlinson-Harashima precoding) should be of interest for suboptimum pre–Rake combining with small number of fingers.

Bibliography

[1] S. Roy, J.R. Foerster, V.S. Somayazulu, and D.G. Leeper. Ultrawideband Radio Design: The Promise of High-Speed, Short-Range Wireless Connectivity. *Proceedings of the IEEE*, 92:295 – 311, February 2004.

[2] H. Arslan, Z.N. Chen, and M.-G. Di Benedetto. *Ultra Wideband Wireless Communication*. John Wiley & Sons, Inc., New York, 2006.

[3] FCC Revision of part 15 of the Commission's Rules Regarding Ultra–Wideband Transmission Systems: Report and Order, February 2002.

[4] FCC First Report and Order: In the Matter of Revision of part 15 of the Commission's Rules Regarding Ultra–Wideband Transmission Systems, April 2002.

[5] S.S. Mo, N. Guo, J.Q. Zhang, and R.C. Qiu. UWB MISO Time Reversal with Energy Detector Receiver Over ISI Channels. *4th IEEE Consumer Communications and Networking Conference (CCNC)*, pages 629 – 633, January 2007.

[6] A.A. D'Amico and L. Taponecco. A Differential Receiver for UWB Systems. *IEEE Transactions on Wireless Communications*, 5:1601 – 1605, July 2006.

[7] A.G. Klein, D.R. Brown, D.L. Goeckel, and C.R.Ir. Johnson. RAKE Reception for UWB Communication Systems with Intersymbol Interference.

4th IEEE Workshop on Signal Processing Advances in Wireless Communications (SPAWC), pages 244 – 248, June 2003.

[8] T.Q.S. Quek and M.Z. Win. Ultrawide Bandwidth Transmitted-Reference Signaling. *IEEE International Conference on Communications*, 6:3409 – 3413, June 2004.

[9] M. Win and R. Scholtz. Impulse Radio: How it Works. *IEEE Commun. Letters*, 2:36–38, February 1998.

[10] M. Win and R. Scholtz. Characterization of Ultra-Wide Bandwidth Wireless Indoor Channels: A Communication-Theoretic View. *IEEE J. Select. Areas Commun.*, 20:1613–1627, December 2002.

[11] R. Esmailzadeh, E. Sourour, and M. Nakagawa. PreRAKE Diversity Combining in Time-Division Duplex CDMA Mobile Communications. *IEEE Trans. Veh. Technol.*, 48:795–801, May 1999.

[12] A. Parvulescu. Matched-Signal ('MESS') Processing by the Ocean. *J. Acoust. Soc. Am.*, 98:943–960, August 1995.

[13] T. Strohmer, M. Emami, J. Hansen, G. Papanicolaou, and A. Paulraj. Application of Time-Reversal with MMSE Equalizer to UWB Communications. In *Proceedings of the IEEE Global Telecomm. Conf. (Globecom)*, pages 3123–3127, November 2004.

[14] S. Imada and T. Ohtsuki. Pre-Rake Diversity Combining for UWB Systems in IEEE 802.15 UWB Multipath Channel. In *Proceedings of the Joint Ultra Wideband Systems and Technology (UWBST) and Intern. Workshop for Ultra Wideband Systems (WIWUWBS)*, pages 236–240, May 2004.

[15] K. Usuda, H. Zhang, and M. Nakagawa. Pre-Rake Performance for Pulse Based UWB System in a Standardized UWB Short-Range Channel. In *Proceedings of the IEEE Wireless Commun. and Networking Conf. (WCNC)*, pages 920–925, March 2004.

[16] N. Guo, R. Qiu, and B. Sadler. An Ultra-Wideband Autocorrelation Demodulation Scheme with Low-Complexity Time Reversal Enhancement. In *Proceedings of the IEEE Military Commun. Conf. (Milcom)*, pages 3066–3072, Atlantic City, October 2005.

[17] H. Nguyen, I. Kovcs, and P. Eggers. A Time Reversal Transmission Approach for Multiuser UWB Communications. *IEEE Trans. Antennas and Propagation*, 54:3216–3224, November 2006.

[18] Y. Nishida, C. Fukao, M. Fujii, M. Itami, and K. Itoh. A Study on Improving Performance of Pre-Post-RAKE Combining in UWB-IR System. In *Proceedings of the IEEE Intern. Conf. Ultra-Wideband (ICUWB)*, pages 79–84, September 2006.

[19] R. Qiu, C. Zhou, N. Guo, and J. Zhang. Time Reversal With MISO for Ultrawideband Communications: Experimental Results. *IEEE Antennas and Wireless Propagation Letters*, 5:269–273, December 2006.

[20] W. Cao, A. Nallanathan, and C. Chai. On the Tradeoff between Data Rate and BER Performance of Pre-RAKE DS UWB System. In *Proceedings of the IEEE Global Telecomm. Conf. (Globecom)*, November 2006.

[21] Y.-H. Chang, S.-H. Tsai, X. Yu, and C.-C. Kuo. Ultrawideband Transceiver Design Using Channel Phase Precoding. *IEEE Trans. Signal Processing*, 55:3807–3822, July 2007.

[22] G. Ding, D. Wang, and Z. Chen. Performance Evaluation of Two Kinds of Precoding Joint with MMSE Equalization in DS–UWB. In *Proceedings of the First Intern. Conf. Commun. and Networking in China (ChinaCom)*, Beijing, October 2006.

[23] M. Eslami and X. Dong. Performance of Rake-MMSE-equalizer for UWB Communications. *IEEE Wireless Communications and Networking Conference*, 2:855 – 860, March 2005.

[24] M. Emami, M. Vu, J. Hansen, A. Paulraj, and G. Papanicolaou. Matched Filtering with Rate Back–off for Low Complexity Communications in Very Large Delay Spread Channels. In *Proceedings of the 38th Asilomar Conf. Signals, Systems, and Computers*, pages 218–222, November 2004.

[25] T. Berger and D.W. Tufts. Optimum Pulse Amplitude Modulation, Part I: Transmitter-Receiver Design and Bounds from Information Theory. *IEEE Trans. Inform. Theory*, IT-13:196–208, 1967.

[26] J. Yang and S. Roy. On Joint Transmitter and Receiver Optimization for Multi–Input Multi–Output (MIMO) Transmission Systems. *IEEE Trans. Commun.*, COM-42:3221–3231, December 1994.

[27] D. Tse and P. Viswanath. *Fundamentals of Wireless Communication*. Cambridge Univeristy Press, Cambridge, 2005.

[28] Y. Ishiyama and T. Ohtsuki. Performance Comparison of UWB-IR Using RAKE Receivers in UWB Channel Models. *International Workshop on Ultra Wideband Systems Joint with Conference on Ultrawideband Systems and Technologies*, pages 226 – 230, May 2004.

[29] Channel Modeling Sub-Committee Final Report. IEEE 802.15-02/368r5-SG3a, IEEE P802.15. December 2002.

[30] A. Molisch, J. Foerster, and M. Pendergrass. Channel Models for Ultrawideband Personal Area Networks. *IEEE Wireless Communications*, 10:14–21, December 2003.

[31] Z. Lin, X. Peng, K. Png, and F. Chin. Kronecker Modelling for Correlated Shadowing in UWB MIMO Channels. In *Proceedings of the IEEE Wireless Commun. and Networking Conf. (WCNC)*, Hong Kong, March 2007.

[32] A. Saleh and R. Valenzuela. A Statistical Model for Indoor Multipath Propagation. *IEEE Journal on Selected Areas in Communications*, 5:128 – 137, February 1987.

[33] J.G. Proakis. *Digital Communications*. McGraw–Hill, New York, forth edition, 2001.

[34] A.V. Oppenheim and A.S. Willsky. *Signals and Systems*. Prentice–Hall, Inc., Upper Saddle River, New Jersey, 1996.

[35] T.K. Moon and W.C. Stirling. *Mathematical Methods and Algorithms for Signal Processing*. Prentice Hall, New York, 2000.

[36] V. Poor and S. Verdu. Probability of Error in MMSE Multiuser Detection. *IEEE Trans. Inform. Theory*, 43:858–871, May 1997.

[37] B. Hu and N. Beaulieu. Comparison of Modulation Schemes and Rake Receiver Structures for UWB Systems on an IEEE 802.15.3 Indoor Channel. In *Proceedings of the IEEE Global Telecommun. Conf. (Globecom)*, pages 3493–3497, November 2005.

[38] F. Ling. Matched Filter–Bound for Time–Discrete Multipath Rayleigh Fading Channels. *IEEE Trans. Commun.*, COM-43:710–713, February–April 1995.

[39] S. Haykin. *Adaptive Filter Theory*. Prentice-Hall, Upper Saddle River, New Jersey, Third Edition, 1996.

[40] I. S. Gradshteyn and I. M .Ryzhik. *Table of Integrals, Series, and Products*. Academic Press, New York, 2000.

[41] R. Fisher, R. Kohno, M. McLaughlin, and M. Welbourn. DS–UWB Physical Layer Submission to IEEE 802.15 Task Group 3a (Doc. Number P802.15-03/0137r4). January 2005.